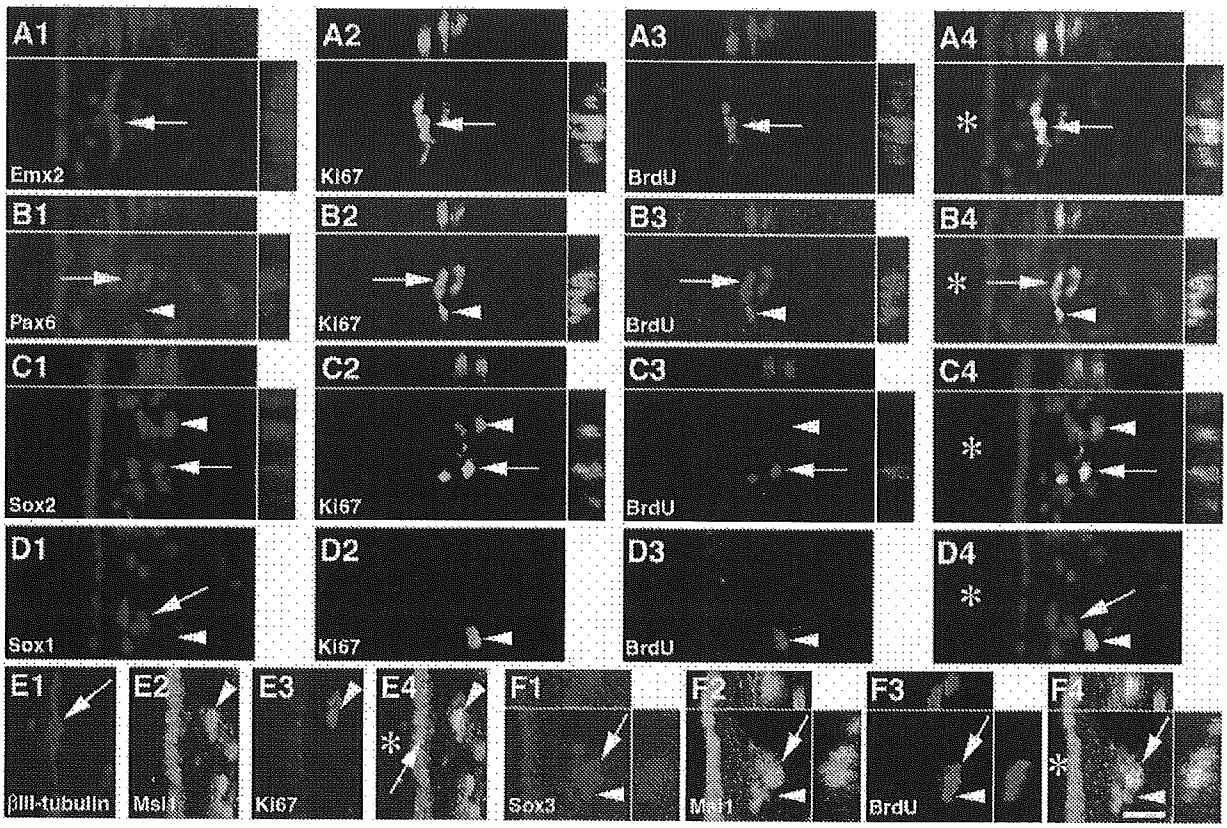

Fig. 4. Transcription factor expression by sustained proliferating progenitors at long-term survival time-points after BrdU. (A) Triple-labeling for Emx2 (A1), Ki67 (A2) and BrdU (A3), and overlay (A4), on day 79. Triple-labeled cells are depicted by an arrow. (B) Triple-labeling for Pax6 (B1), Ki67 (B2) and BrdU (B3), and overlay (B4), on day 79. Triple-labeled cells are depicted by an arrow, a $Pax6^{-}$/Ki67 /$BrdU^{+}$ cell is shown by an arrowhead. (C) Triple-labeling for Sox2 (C1), Ki67 (C2) and BrdU (C3), and overlay (C4), on day 79. Triple-labeled cells are depicted by an arrow, a $Sox2^{+}$/$Ki67^{+}$/$BrdU^{-}$ cell is shown by an arrowhead. Sox2 staining is representative also for Sox3. (D) Triple-labeling for Sox1 (D1), Ki67 (D2) and BrdU (D3), and overlay (D4), on day 79. Note lack of Sox1 expression (arrow) by a $Ki67^{+}$/$BrdU^{+}$ cell (arrowhead). (E) Triple-labeling for βIII-tubulin (E1) Musashi1 (Msi1, E2), Ki67 (E3), and overlay (E4), on day 44. Ki67 co-labels with Msi1 (arrowheads), not with βIII-tubulin (arrows). (F) Triple-labeling for Sox3 (F1), Musashi1 (F2) and BrdU (F3), and overlay (F4), on day 79. Triple-stained cells are depicted by arrows. Scale bar=20 μm. Asterisk, lateral ventricle.

Olig2, Olig3 or Nkx2.2, data not shown) co-labeled with Ki67 (Fig. 6I).

DISCUSSION

Mechanisms that specify the fate of embryonic neural precursors might be at least in part recapitulated in the adult brain (Gotz, 2003; Alvarez-Buylla and Lim, 2004). This concept was supported by data in rodents showing that transcriptional regulators of embryonic precursors were also expressed by adult SVZa progenitors: Pax6 and Olig2 (Hack et al., 2004), Emx2 (Galli et al., 2002), Dlx2 (Doetsch et al., 2002), and Sox2 (Ferri et al., 2004; Komitova and Eriksson, 2004). We first report expression of developmentally-regulated transcription factors at protein level by SVZa progenitor cells of adult primate brain. Ischemia increased the absolute numbers of $BrdU^{+}$ cells expressing the proteins Pax6, Emx2, Sox1–3, Ngn1, Dlx1,5, Olig1,3, and Nkx2.2 as compared with controls (Fig. 8A). The decrease of BrdU/transcription factor co-labeled cells at long-term as compared with short-term time intervals reflects the global decrease of labeled progenitor cells in SVZa over time (Tonchev et al., 2005) as the precursor cells migrate away from SVZa toward the olfactory bulb. Notably, ischemia did not affect the percentage of BrdU/transcription factor double-labeled cells as compared with controls. These data are compatible with our previous

by an arrow) and Doublecortin (DCX) (D2; arrowheads), and overlay (D3), on day 23. (E) Double-staining for Sox1 (E1, arrow depicts a positive cluster) and Musashi1 (E2; arrowhead), and overlay (E3), on day 44. (F) Double-staining for Sox1 (F1) and βIII-tubulin (F2), and overlay (F3), on day 44 (the cluster depicted by an arrow is reconstructed in the *x* and *y* axes, on left and top the image). (G) Double-staining for Sox2 (G1) and GFAP (G2), and overlay (G3), on day 9. (H) Percentages of $Pax6^{+}$ (H1), $Emx2^{+}$ (H2), $Sox2,3^{+}$ (H3) and $Sox1^{+}$ (H4) cells co-expressing Musashi1 or βIII-tubulin in the postischemic monkeys. Transcription factor-positive cells that were $Musashi1^{-}$/βIII-$tubulin^{-}$ are designated "other." Percentages in the control monkeys did not differ significantly from the postischemic ones. Scale bar=50 μm (A–C); 10 μm (D–G). Asterisk, lateral ventricle.

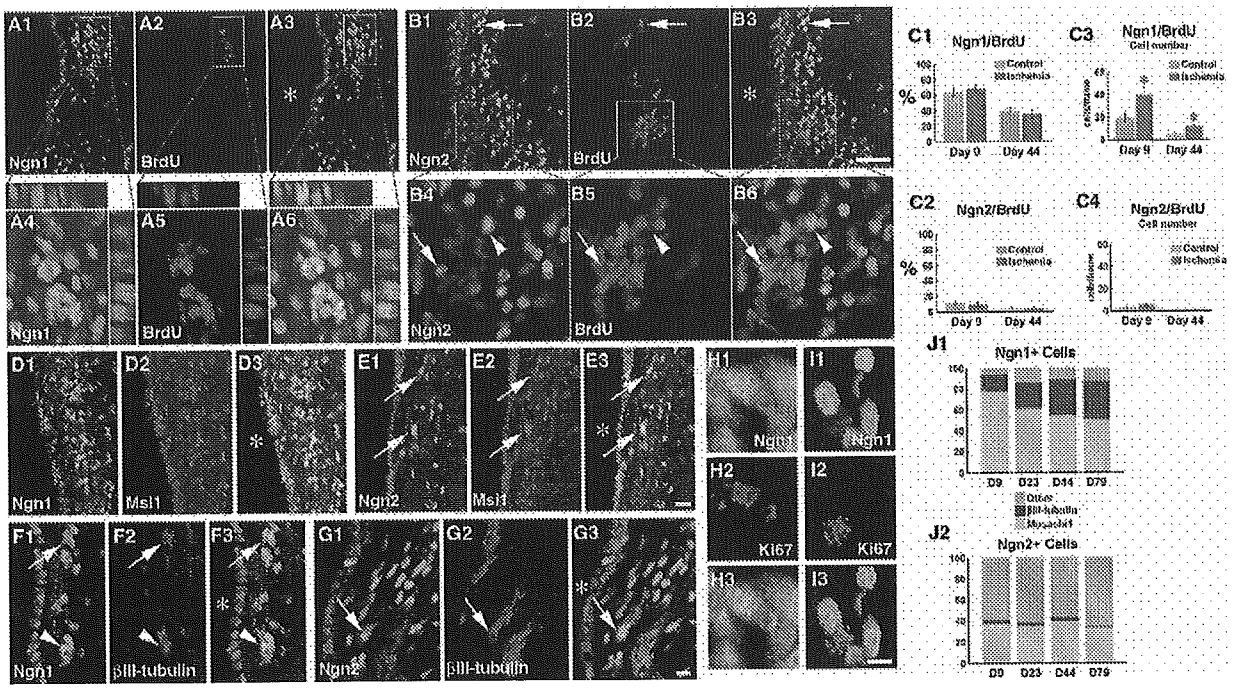

Fig. 5. Expression of Ngn proteins by SVZa progenitor cells. (A) Double-staining for Ngn1 (A1) and BrdU (A2), and overlay (A3), on day 9. The region depicted by a box is magnified in A4–A6 with orthogonal projections. (B) Double-staining for Ngn2 (B1) and BrdU (B2), and overlay (B3), on day 9. Double-labeled cells (arrow) are rare. The region depicted by a box is magnified in B4–B6 with orthogonal projections. Note a single Ngn2$^+$/BrdU$^+$ cell (arrow) within the BrdU$^+$ cluster; a Ngn2$^+$/BrdU$^-$ cell (arrowhead) is entangled in the same aggregate. (C) Percentages (C1, C2) and absolute numbers (C3, C4) of BrdU$^+$Ngn1$^+$ (C1, C3) and BrdU$^+$/Ngn2$^+$ cells (C2, C4). * $P<0.05$ versus control. (D) Double-staining for Ngn1 (D1) and Musashi1 (Msi1, D2), and overlay (D3), on day 9. Note extensive co-labeling of the two signals. (E) Double-staining for Ngn2 (E1) and Musashi1 (E2), and overlay (E3), on day 9. The Ngn2$^+$/Musashi1$^+$ cells (arrows) are rare. (F) Double-staining for Ngn1 (F1) and βIII-tubulin (F2), and overlay (F3), on day 23. A Ngn1$^+$ "doublet" is double-labeled (arrow), and a single cell of an Ngn1$^+$ cluster (arrowhead) expresses βIII-tubulin, while a neighboring βIII-tubulin$^+$ cell is negative for Ngn1. (G) Double-staining for Ngn2 (G1) and βIII-tubulin (G2), and overlay (G3), on day 44. A single Ngn2$^+$ cells is double-labeled (arrow). (H) Double-staining for Ngn1 (H1) and Ki67 (H2), and overlay (H3), on day 9. (I) Double-staining for Ngn1 (I1) and Ki67 (I2), and overlay (I3), on day 44. (J) Percentages of Ngn1$^+$ (J1) or Ngn2$^+$ (J2), cells co-expressing Musashi1 or βIII-tubulin in the postischemic monkeys. Transcription factor-positive cells that were Musashi1$^-$/βIII-tubulin$^-$ are designated "other." Percentages in the control monkeys did not differ significantly from the postischemic ones. Scale bar=50 μm (A, B); 20 μm (D, E); 10 μm (F, G); 5 μm (H, I). Asterisk, lateral ventricle.

results showing no change in the percentage of BrdU/Musashi1 or BrdU/βIII-tubulin co-labeling between postischemic and control SVZa (Tonchev et al., 2005). Altogether, our findings suggest that ischemia increases the progenitor cell proliferation and absolute numbers without affecting progenitor differentiation, and in particular neuronal differentiation.

Despite the decrease of progenitors in SVZa over time, a significant proportion of these cells remained in SVZa for at least three months after ischemia (Tonchev et al., 2005). Immunophenotype analysis of these sustained cells revealed two distinct cell populations, each with a characteristic transcription factor expression pattern at protein level (Fig. 8B). The segregation of transcriptional regulators expressed by adult monkey neural or neuronal progenitors (Fig. 8B) suggests that a set of transcription factors might define a specific cell phenotype, similarly to the developing brain. Notably, the localization of some of the examined factors in either neuronal (βIII-tubulin$^+$) or neural (Musashi1$^+$) precursors was not strictly selective as cells positive for Dlx1,5, Ngn1, Nkx2.2 or Olig3 were co-labeled not only for βIII-tubulin, but also for Musashi1. At the same time, these cells were negative for Ki67 at long-term time-points, indicating that the Musashi1$^+$ cells co-labeled for Dlx1,5, Ngn1, Nkx2.2 or Olig3 at long-term time points were non-mitotic cells. These could be quiescent progenitors not in active cell cycle at the time of animal perfusion. Accordingly, we have previously demonstrated that Musashi1$^+$/GFAP$^+$ cells in SVZa are not in active cell cycle (Tonchev et al., 2005), and a GFAP-enriched cellular population is thought to contain neural stem cells in adult human SVZa (Sanai et al., 2004). The partly overlapping transcription factor expression between Musashi1$^+$ and βIII-tubulin$^+$ progenitors might be due to common molecular mechanisms involved in their regulation and/or might result from a lineage relationship between these two cell types. Further experiments are needed to clarify whether any of these possibilities might be true.

Different from Dlx1,5, Ngn1, Nkx2.2 or Olig3, the transcription factor Sox1 co-stained exclusively with βIII-tubulin. While the high Sox1/βIII-tubulin co-labeling is consistent with high Sox1/BrdU and BrdU/βIII-tubulin co-labeling (Tonchev et al., 2005) at long-term time points, the relatively high percentage of BrdU$^+$ cells co-stained for Sox1 (about 50%) at the short-term (day 9) time-point with concomitant minimal Sox1/Musashi1 co-staining (<3%) is dis-

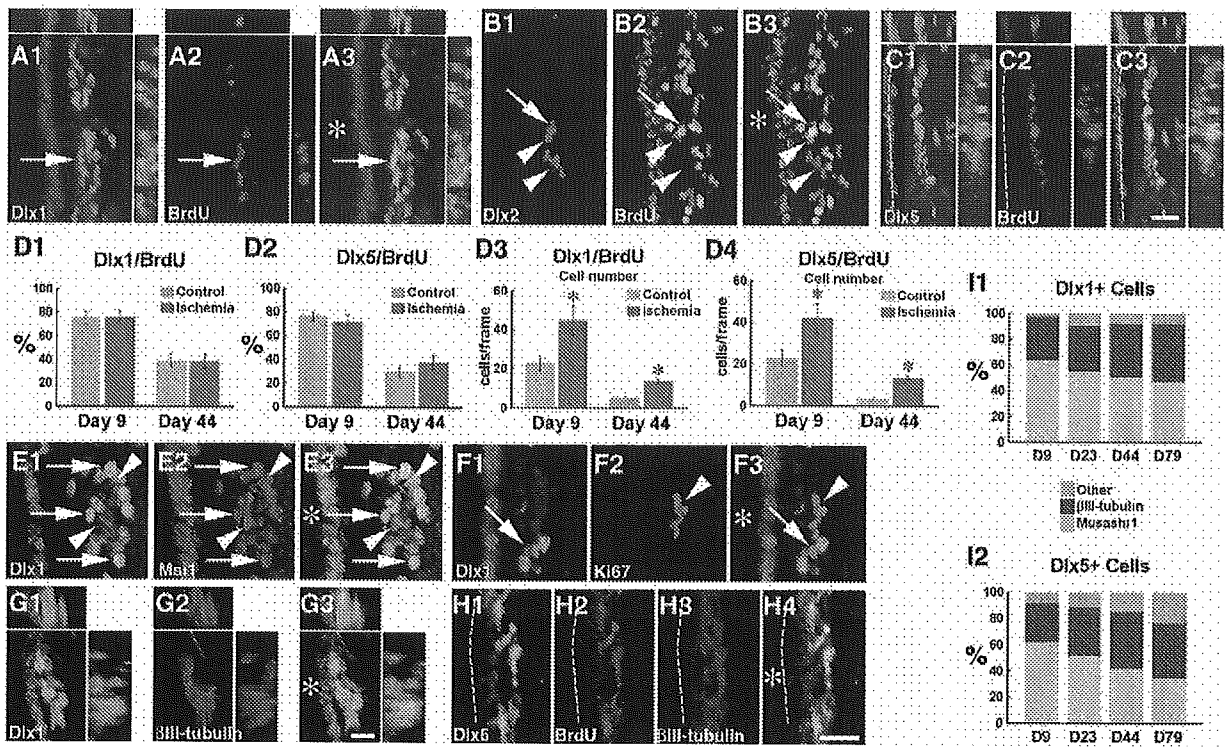

Fig. 6. Expression of Dlx proteins by SVZa progenitor cells. (A) Double-staining for Dlx1 (A1) and BrdU (A2), and overlay (A3), on day 9. A double-positive cluster is depicted (arrow). (B) Double-staining for Dlx2 (B1) and BrdU (B2), and overlay (B3), on day 9. Note that Dlx2$^+$ cells (arrows) do not co-label with BrdU (arrowheads). (C) Double-staining for Dlx5 (C1) and BrdU (C2), and overlay (C3), on day 9. (D) Percentages (D1, D2) and absolute numbers (D3, D4) of BrdU$^+$/Dlx1$^+$ (D1, D3) and BrdU$^+$/Dlx5$^+$ (D2, D4) cells. * $P<0.05$ versus control. (E) Double-staining for Dlx1 (E1) and Musashi1 (Msi1, E2), and overlay (E3), on day 9. Note double-positive cells (e.g. arrows), and Dlx1$^-$/Musashi1$^+$ cells exhibiting mitotic figures (arrowheads), entangled in a cluster. (F) Double-staining for Dlx1 (F1, arrows) and Ki67 (F2, arrowheads), and overlay (F3), on day 44. (G) Double-staining for Dlx1 (G1) and βIII-tubulin (G2), and overlay (G3), on day 79. The Dlx1$^+$ cluster is co-stained by βIII-tubulin. (H) Triple-staining for Dlx5 (H1), BrdU (H2) and βIII-tubulin (H3), and overlay (H4), on day 44. Note co-labeling in (ependymal layer is outlined by a dotted line). (I) Percentages of Dlx1$^+$ (I1) or Dlx5$^+$ (I2), cells co-expressing Musashi1 or βIII-tubulin in the postischemic monkeys (for Dlx2 see text). Transcription factor-positive cells that were Musashi1$^-$/βIII-tubulin$^-$ are designated "other." Percentages in the control monkeys did not differ significantly from the postischemic ones. Scale bar=20 μm (A–C, H); 10 μm (E–G). Asterisk, lateral ventricle.

cordant with the high BrdU/Musashi1 co-expression characteristic for day 9 (Tonchev et al., 2005). The following cell phenotypes could be BrdU$^+$/Sox1$^+$/Musashi1$^-$ cells on day 9: (*i*) the nearly 30% of the BrdU$^+$ cells negative for Musashi1 on day 9 (Tonchev et al., 2005), and (*ii*) the approximately 10% of the Sox1$^+$ cells with an unidentified (non-βIII-tubulin/non-Musashi1) phenotype as shown in the present study. Moreover, the finding of cells stained for transcription factors but negative for either βIII-tubulin or Musashi1 suggests phenotypical heterogeneity, a feature that is observed in multipotent progenitor cells (Pevny and Rao, 2003).

Non-primate mammalian models are essential in addressing fundamental stem cell issues. At the same time, primates appear to exhibit considerably lower levels of neurogenesis than non-primate mammals at both normal conditions (Kornack and Rakic, 1999) or in a context of injury-enhanced neurogenic response (Tonchev et al., 2003). The framework of molecular signals that may underlie this interspecies discrepancy is currently unknown. We observed certain similarities between our results in monkeys and studies using non-primate models with respect to transcription factor expression by adult SVZa progenitors. In particular, Emx2 and Sox2,3 were expressed by actively dividing sustained progenitors in monkey SVZa consistent with their previously reported expression in early multipotent progenitor/stem cells (Galli et al., 2002; Bylund et al., 2003; Graham et al., 2003; Ferri et al., 2004; Komitova and Eriksson, 2004), while Sox1 (but not Sox2,3) protein was predominantly localized in monkey neuronal progenitors consistent with its previously reported activity inducing neuronal commitment (Kan et al., 2004). At the same time, we noticed the following discrepancies between our results in monkeys and studies using non-primate animal models. First, Pax6 appeared to be predominantly localized to neuronal progenitors in adult mouse SVZa (Hack et al., 2004), while in monkey SVZa Pax6 was mainly positive in neural progenitors. Second, the transcription factors Dlx2 and Olig2 label transit-amplifying precursors in adult rodent SVZa (Doetsch et al., 2002; Hack et al., 2004) which are highly prolifera-

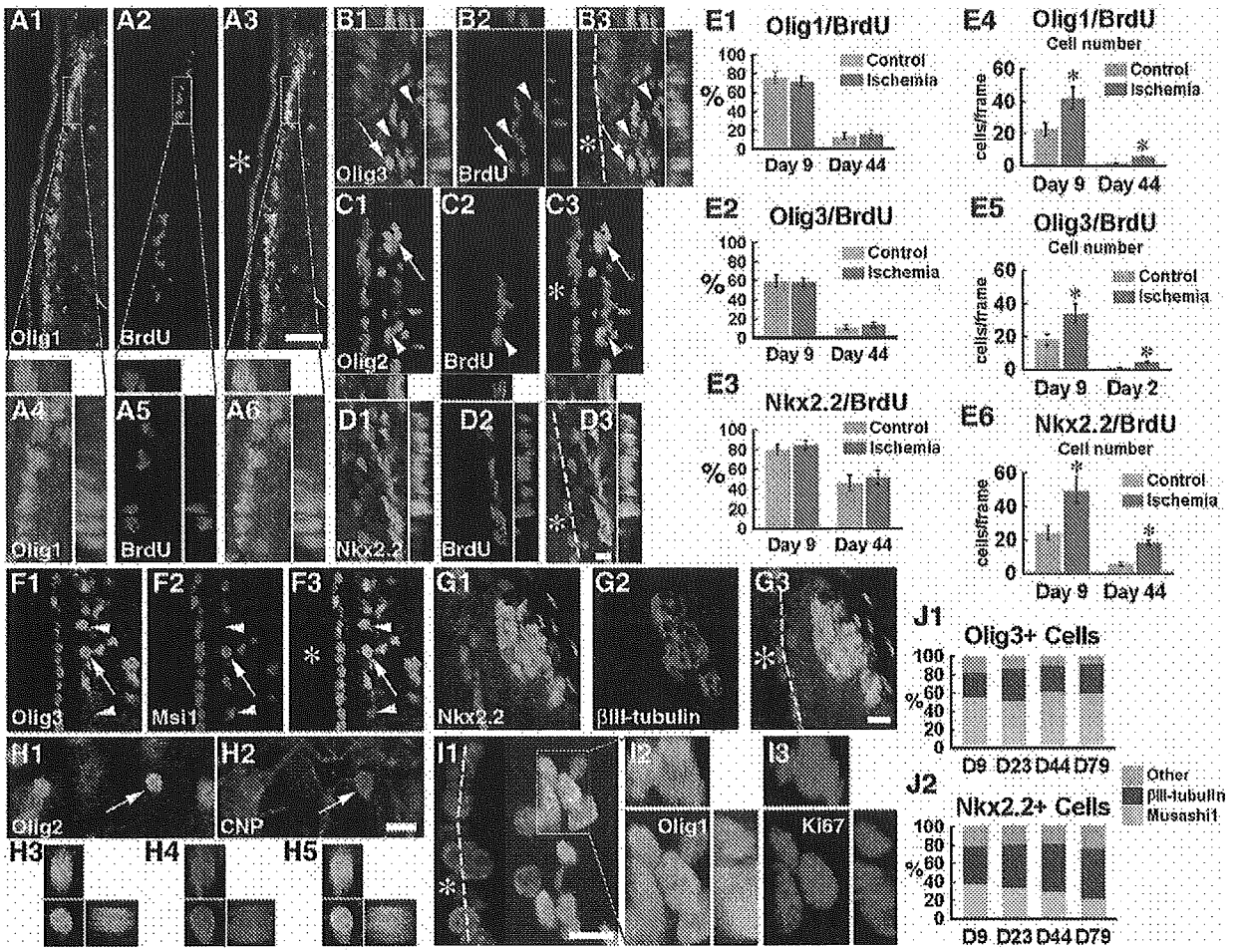

Fig. 7. Expression of Olig proteins and Nkx2.2 by SVZa progenitor cells. (A) Double-staining for Olig1 (A1) and BrdU (A2), and overlay (A3), on day 9. The region depicted by a box is magnified in A4–A6 with orthogonal projections. (B) Double-staining for Olig3 (B1) and BrdU (B2), and overlay (B3), on day 44. Several $BrdU^+$ cells are $Olig3^-$ (arrowheads). A double-positive cell is depicted by arrows. (C) Double-staining for Olig2 (C1) and BrdU (C2), and overlay (C3), on day 9. A cluster positive for Olig2 (arrows) is not co-labeled by BrdU. A single cell in a neighboring $BrdU^+$ cluster is weakly positive for Olig2 (arrowheads). (D) Double-staining for Nkx2.2 (D1) and BrdU (D2), and overlay (D3), on day 9. Most cells are double-positive. (E) Percentages (E1–E3) and absolute numbers (E4–E6) of $BrdU^+/Olig1^+$ (E1, E4), $BrdU^+/Olig3^+$ (E2, E5) and Nkx2.2 (E3, E6). * $P<0.05$ versus control. (F) Double-staining for Olig3 (F1) and Musashi1 (Msi1, F2), and overlay (F3), on day 9 (representative also for Olig1 and Nkx2.2). Double-labeled cells are depicted by arrows, while single-labeled cells (either $Olig3^+/Musashi1^-$ or $Olig3^-/Musashi1^+$) are depicted by arrowheads. (G) Double-staining for Nkx2.2 (G1) and βIII-tubulin (G2), and overlay (G3), on day 23 (representative also for Olig3). (H) Staining for Olig2 (H1) and CNP (H2), on day 79. Two CNP^+ oligodendrocytes are co-labeled by Olig2. The cell depicted by an arrow is shown in a three-dimensional view with color separation in H3 (Olig2), H4 (CNP) and H5 (overlay). The image is representative also for Nkx2.2. (I) Double-staining for Olig1 (I1) and Ki67 (I2), on day 44. The cluster depicted by a box is magnified in I2 and I3 with color separation and orthogonal projections. (J) Percentages of $Olig3^+$ (J1) or $Nkx2.2^+$ (J2), cells co-expressing Musashi1 or βIII-tubulin in the postischemic monkeys (for Olig1,2 see text). Transcription factor-positive cells that were $Musashi1^-/βIII\text{-}tubulin^-$ are designated "other." Percentages in the control monkeys did not differ significantly from the postischemic ones. Scale bar=50 μm (A); 10 μm (B–I). Asterisk, lateral ventricle.

tive (Doetsch et al., 1997), while in our experiments we found very few $BrdU^+/Dlx2^+$ or $BrdU^+/Olig2^+$ cells. This suggests that monkey SVZa niche either has very few type C cells or that these cells do not express Dlx2 and Olig2. A detailed characterization of the cellular composition of adult monkey SVZa as done in rodents (Doetsch et al., 1997) is necessary to confirm or put aside this speculation.

The decision whether monkey SVZa progenitors will preserve their localization in the niche or will migrate away from SVZa might be coordinated by a balance of factors promoting or inhibiting proliferation and migration. Such putative factors are the neurotransmitters glutamate and GABA, which exhibit either stimulatory or inhibitory effects on the proliferation of embryonic precursor cells from ventricular zone or SVZ, respectively (Haydar et al., 2000). This suggests that distinct precursor cell populations respond to glutamate/GABA in different ways. In adult SVZa, glutamate and GABA have been reported to exert opposing effects on progenitor cells: glutamate activates (Brazel et al., 2005) while GABA inhibits (Liu et al., 2005) their proliferation. There-

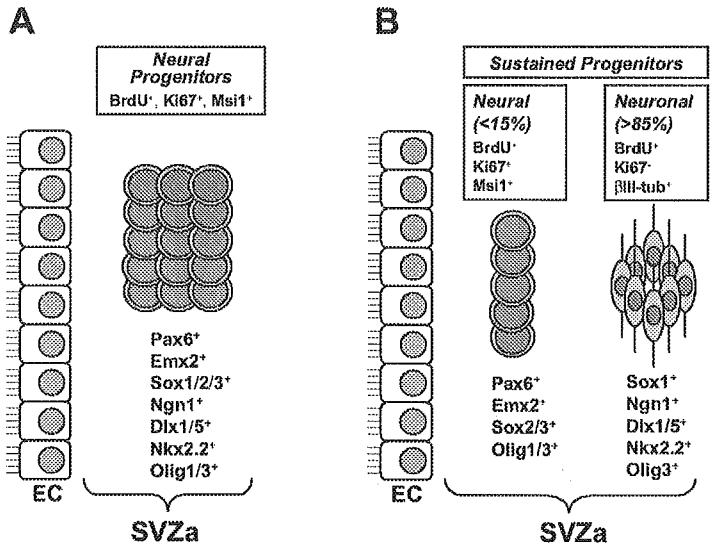

Fig. 8. Schematic summary of transcription factor protein expression by monkey SVZa progenitor cells in the short-term (A) or long-term (B) survival time-points after ischemia. (A) On day 9 the $BrdU^+$ cells are predominantly positive for Musashi1 and Ki67 (Tonchev et al., 2005). These cells expressed a large number of the transcription factors investigated in this study (Ngn2, Dlx2 and Olig2 were omitted from the scheme because of the minimal proportion of co-labeling with BrdU; a small fraction of $BrdU^+/\beta III\text{-tubulin}^+$ cells at this time point were also skipped for clarity). (B) At long-term after ischemia, the sustained $BrdU^+$ cells are either $Musashi1^+/Ki67^+$ (up to 15% of the $BrdU^+$ cells) or $\beta III\text{-tubulin}^+/Ki67^-$ (over 85% of the $BrdU^+$ cells) (Tonchev et al., 2005), and these two distinct cell phenotypes expressed distinct sets of transcription factor proteins. The sustained cells in active cell cycle ($Ki67^+$) preferentially expressed markers for early stem/progenitor cells (Emx2, Pax6, Sox2,3), while sustained cells that have exited active cell cycle ($Ki67^-$) were preferentially positive for region-specific proteins with pro-neuronal actions (Sox1, Dlx1,5, Ngn1, Nkx2.2). Note that Sox1, Ngn1, Dlx1,5, Nkx2.2 and Olig3 proteins were expressed also by some $Musashi1^+$ cells (see text for details), which is not depicted on the scheme, for clarity. EC, ependymal cells; Msi1, Musashi1; βIII-tub, βIII-tubulin.

fore, it is possible to speculate that these two endogenous amino acids may differentially affect neural or neuronal progenitors in monkey SVZa to achieve precursor cell proliferation/differentiation with either retention in SVZa or migration toward the olfactory bulb. Other extracellular signaling molecules might also be involved in precursor cell modulation by affecting transcription factor activity. For example, Ngn1 is required for erythropoietin-enhanced neurogenesis (Wang et al., 2006).

The present study had not aimed at deciphering the mechanisms for differential expression of transcription factors by neural progenitors with different proliferation or migration activities. Such mechanisms possibly include modulatory effects at promoter and/or enhancer regions of various transcription factors. For example, two distinct Sox2 enhancers are active in multipotent neural progenitors but cease to function in differentiated cells (Zappone et al., 2000; Miyagi et al., 2004). The mouse Pax6 gene has three promoters under the control of at least six different enhancers, directing Pax6 expression in distinct tissues (reviewed by Morgan, 2004). Given that different tissues, and even different progenitor cell types, require activation of selective regulatory elements, one may speculate that ischemia could differentially activate such elements in sustained or migrating SVZa progenitors. Unraveling the transcriptional network involved in the regulation of adult progenitor cell specification may lead to development of more effective strategies to direct these cells to adopt a selective cellular phenotype required in a specific brain lesion.

Acknowledgments—We thank Hirohide Takebayashi for the anti-Olig2 antibody and George N. Chaldakov for valuable discussions. The Japanese Ministries of Education, Culture, Sports, Science and Technology (Kiban B: 15390432) and Health, Labor and Welfare (H15-Kokoro-018), and the Bulgarian Ministry of Education and Science (L1311/03) supported this work.

REFERENCES

Alvarez-Buylla A, Lim DA (2004) For the long run: maintaining germinal niches in the adult brain. Neuron 41:683–686.

Anderson SA, Qiu M, Bulfone A, Eisenstat DD, Meneses J, Pedersen R, Rubenstein JL (1997) Mutations of the homeobox genes Dlx-1 and Dlx-2 disrupt the striatal subventricular zone and differentiation of late born striatal neurons. Neuron 19:27–37.

Arvidsson A, Collin T, Kirik D, Kokaia Z, Lindvall O (2002) Neuronal replacement from endogenous precursors in the adult brain after stroke. Nat Med 8:963–970.

Braun PE, Sandillon F, Edwards A, Matthieu JM, Privat A (1988) Immunocytochemical localization by electron microscopy of 2′3′-cyclic nucleotide 3′-phosphodiesterase in developing oligodendrocytes of normal and mutant brain. J Neurosci 8:3057–3066.

Brazel CY, Nunez JL, Yang Z, Levison SW (2005) Glutamate enhances survival and proliferation of neural progenitors derived from the subventricular zone. Neuroscience 131:55–65.

Bylund M, Andersson E, Novitch BG, Muhr J (2003) Vertebrate neurogenesis is counteracted by Sox1–3 activity. Nat Neurosci 6:1162–1168.

Doetsch F, Garcia-Verdugo JM, Alvarez-Buylla A (1997) Cellular composition and three-dimensional organization of the subventricular germinal zone in the adult mammalian brain. J Neurosci 17: 5046–5061.

Doetsch F, Petreanu L, Caille I, Garcia-Verdugo JM, Alvarez-Buylla A (2002) EGF converts transit-amplifying neurogenic precursors in the adult brain into multipotent stem cells. Neuron 36:1021–1034.

Eriksson PS, Perfilieva E, Bjork-Eriksson T, Alborn AM, Nordborg C, Peterson DA, Gage FH (1998) Neurogenesis in the adult human hippocampus. Nat Med 4:1313–1317.

Fancy SP, Zhao C, Franklin RJ (2004) Increased expression of Nkx2.2 and Olig2 identifies reactive oligodendrocyte progenitor cells responding to demyelination in the adult CNS. Mol Cell Neurosci 27:247–254.

Ferri AL, Cavallaro M, Braida D, Di Cristofano A, Canta A, Vezzani A, Ottolenghi S, Pandolfi PP, Sala M, DeBiasi S, Nicolis SK (2004) Sox2 deficiency causes neurodegeneration and impaired neurogenesis in the adult mouse brain. Development 131:3805–3819.

Gage FH (2000) Mammalian neural stem cells. Science 287:1433–1438.

Galli R, Fiocco R, De Filippis L, Muzio L, Gritti A, Mercurio S, Broccoli V, Pellegrini M, Mallamaci A, Vescovi AL (2002) Emx2 regulates the proliferation of stem cells of the adult mammalian central nervous system. Development 129:1633–1644.

Gleeson JG, Lin PT, Flanagan LA, Walsh CA (1999) Doublecortin is a microtubule-associated protein and is expressed widely by migrating neurons. Neuron 23:257–271.

Gotz M (2003) Glial cells generate neurons-master control within CNS regions: developmental perspectives on neural stem cells. Neuroscientist 9:379–397.

Graham V, Khudyakov J, Ellis P, Pevny L (2003) SOX2 functions to maintain neural progenitor identity. Neuron 39:749–765.

Hack MA, Sugimori M, Lundberg C, Nakafuku M, Gotz M (2004) Regionalization and fate specification in neurospheres: the role of Olig2 and Pax6. Mol Cell Neurosci 25:664–678.

Haydar TF, Wang F, Schwartz ML, Rakic P (2000) Differential modulation of proliferation in the neocortical ventricular and subventricular zones. J Neurosci 20:5764–5774.

Heins N, Cremisi F, Malatesta P, Gangemi RM, Corte G, Price J, Goudreau G, Gruss P, Gotz M (2001) Emx2 promotes symmetric cell divisions and a multipotential fate in precursors from the cerebral cortex. Mol Cell Neurosci 18:485–502.

Heins N, Malatesta P, Cecconi F, Nakafuku M, Tucker KL, Hack MA, Chapouton P, Barde YA, Gotz M (2002) Glial cells generate neurons: the role of the transcription factor Pax6. Nat Neurosci 5:308–315.

Iwai M, Sato K, Kamada H, Omori N, Nagano I, Shoji M, Abe K (2003) Temporal profile of stem cell division, migration, and differentiation from subventricular zone to olfactory bulb after transient forebrain ischemia in gerbils. J Cereb Blood Flow Metab 23:331–341.

Jin K, Minami M, Lan JQ, Mao XO, Batteur S, Simon RP, Greenberg DA (2001) Neurogenesis in dentate subgranular zone and rostral subventricular zone after focal cerebral ischemia in the rat. Proc Natl Acad Sci U S A 98:4710–4715.

Kan L, Israsena N, Zhang Z, Hu M, Zhao LR, Jalali A, Sahni V, Kessler JA (2004) Sox1 acts through multiple independent pathways to promote neurogenesis. Dev Biol 269:580–594.

Kaneko Y, Sakakibara S, Imai T, Suzuki A, Nakamura Y, Sawamoto K, Ogawa Y, Toyama Y, Miyata T, Okano H (2000) Musashi1: an evolutionally conserved marker for CNS progenitor cells including neural stem cells. Dev Neurosci 22:139–153.

Komitova M, Eriksson PS (2004) Sox-2 is expressed by neural progenitors and astroglia in the adult rat brain. Neurosci Lett 369: 24–27.

Kornack DR, Rakic P (1999) Continuation of neurogenesis in the hippocampus of the adult macaque monkey. Proc Natl Acad Sci U S A 96:5768–5773.

Kornack DR, Rakic P (2001) The generation, migration, and differentiation of olfactory neurons in the adult primate brain. Proc Natl Acad Sci U S A 98:4752–4757.

Letinic K, Zoncu R, Rakic P (2002) Origin of GABAergic neurons in the human neocortex. Nature 417:645–649.

Liu X, Wang Q, Haydar TF, Bordey A (2005) Nonsynaptic GABA signaling in postnatal subventricular zone controls proliferation of GFAP-expressing progenitors. Nat Neurosci 8:1179–1187.

Miyagi S, Saito T, Mizutani K, Masuyama N, Gotoh Y, Iwama A, Nakauchi H, Masui S, Niwa H, Nishimoto M, Muramatsu M, Okuda A (2004) The Sox-2 regulatory regions display their activities in two distinct types of multipotent stem cells. Mol Cell Biol 24: 4207–4220.

Monuki ES, Walsh CA (2001) Mechanisms of cerebral cortical patterning in mice and humans. Nat Neurosci 4(Suppl):1199–1206.

Morgan R (2004) Conservation of sequence and function in the Pax6 regulatory elements. Trends Genet 20:283–287.

Muzio L, DiBenedetto B, Stoykova A, Boncinelli E, Gruss P, Mallamaci A (2002) Conversion of cerebral cortex into basal ganglia in Emx2(−/−) Pax6(Sey/Sey) double-mutant mice. Nat Neurosci 5:737–745.

Okano H (2002) The stem cell biology of the central nervous system. J Neurosci Res 69:698–707.

Ourednik V, Ourednik J, Flax JD, Zawada WM, Hutt C, Yang C, Park KI, Kim SU, Sidman RL, Freed CR, Snyder EY (2001) Segregation of human neural stem cells in the developing primate forebrain. Science 293:1820–1824.

Parent JM, Vexler ZS, Gong C, Derugin N, Ferriero DM (2002) Rat forebrain neurogenesis and striatal neuron replacement after focal stroke. Ann Neurol 52:802–813.

Pencea V, Bingaman KD, Freedman LJ, Luskin MB (2001) Neurogenesis in the subventricular zone and rostral migratory stream of the neonatal and adult primate forebrain. Exp Neurol 172:1–16.

Perera M, Merlo GR, Verardo S, Paleari L, Corte G, Levi G (2004) Defective neuronogenesis in the absence of Dlx5. Mol Cell Neurosci 25:153–161.

Pevny L, Rao MS (2003) The stem-cell menagerie. Trends Neurosci 26:351–359.

Pincus DW, Keyoung HM, Harrison-Restelli C, Goodman RR, Fraser RA, Edgar M, Sakakibara S, Okano H, Nedergaard M, Goldman SA (1998) Fibroblast growth factor-2/brain-derived neurotrophic factor-associated maturation of new neurons generated from adult human subependymal cells. Ann Neurol 43:576–585.

Rowitch DH (2004) Glial specification in the vertebrate neural tube. Nat Rev Neurosci 5:409–419.

Roy NS, Benraiss A, Wang S, Fraser RA, Goodman R, Couldwell WT, Nedergaard M, Kawaguchi A, Okano H, Goldman SA (2000) Promoter-targeted selection and isolation of neural progenitor cells from the adult human ventricular zone. J Neurosci Res 59:321–331.

Sakakibara S, Imai T, Hamaguchi K, Okabe M, Aruga J, Nakajima K, Yasutomi D, Nagata T, Kurihara Y, Uesugi S, Miyata T, Ogawa M, Mikoshiba K, Okano H (1996) Mouse-Musashi-1, a neural RNA-binding protein highly enriched in the mammalian CNS stem cell. Dev Biol 176:230–242.

Sakakibara S, Okano H (1997) Expression of neural RNA-binding proteins in the postnatal CNS: implications of their roles in neuronal and glial cell development. J Neurosci 17:8300–8312.

Sanai N, Tramontin AD, Quinones-Hinojosa A, Barbaro NM, Gupta N, Kunwar S, Lawton MT, McDermott MW, Parsa AT, Manuel-Garcia Verdugo J, Berger MS, Alvarez-Buylla A (2004) Unique astrocyte ribbon in adult human brain contains neural stem cells but lacks chain migration. Nature 427:740–744.

Schuurmans C, Guillemot F (2002) Molecular mechanisms underlying cell fate specification in the developing telencephalon. Curr Opin Neurobiol 12:26–34.

Schuurmans C, Armant O, Nieto M, Stenman JM, Britz O, Klenin N, Brown C, Langevin LM, Seibt J, Tang H, Cunningham JM, Dyck R, Walsh C, Campbell K, Polleux F, Guillemot F (2004) Sequential phases of cortical specification involve Neurogenin-dependent and -independent pathways. EMBO J 23:2892–2902.

Shirasaki R, Pfaff SL (2002) Transcriptional codes and the control of neuronal identity. Annu Rev Neurosci 25:251–281.

Stenman J, Toresson H, Campbell K (2003) Identification of two distinct progenitor populations in the lateral ganglionic eminence: implications for striatal and olfactory bulb neurogenesis. J Neurosci 23:167–174.

Tonchev AB, Yamashima T, Zhao L, Okano HJ, Okano H (2003) Proliferation of neural and neuronal progenitors after global brain ischemia in young adult macaque monkeys. Mol Cell Neurosci 23:292–301.

Tonchev AB, Yamashima T, Sawamoto K, Okano H (2005) Enhanced proliferation of progenitor cells in the subventricular zone and limited neuronal production in the striatum and neocortex of adult macaque monkeys after global cerebral ischemia. J Neurosci Res 81:776–788.

Wang L, Zhang ZG, Zhang RL, Jiao ZX, Wang Y, Pourabdollah-Nejad DS, Letourneau Y, Gregg SR, Chopp M (2006) Neurogenin 1 mediates erythropoietin enhanced differentiation of adult neural progenitor cells. J Cereb Blood Flow Metab [Epub ahead of print] doi: 10.1038/sj.jcbfm.9600215.

Yamashima T, Kohda Y, Tsuchiya K, Ueno T, Yamashita J, Yoshioka T, Kominami E (1998) Inhibition of ischaemic hippocampal neuronal death in primates with cathepsin B inhibitor CA-074: a novel strategy for neuroprotection based on 'calpain-cathepsin hypothesis.' Eur J Neurosci 10:1723–1733.

Yamashima T (2000) Implication of cysteine proteases calpain, cathepsin and caspase in ischemic neuronal death of primates. Prog Neurobiol 62:273–295.

Zappone MV, Galli R, Catena R, Meani N, De Biasi S, Mattei E, Tiveron C, Vescovi AL, Lovell-Badge R, Ottolenghi S, Nicolis SK (2000) Sox2 regulatory sequences direct expression of a (beta)-geo transgene to telencephalic neural stem cells and precursors of the mouse embryo, revealing regionalization of gene expression in CNS stem cells. Development 127:2367–2382.

Zhang RL, Zhang ZG, Zhang L, Chopp M (2001) Proliferation and differentiation of progenitor cells in the cortex and the subventricular zone in the adult rat after focal cerebral ischemia. Neuroscience 105:33–41.

(Accepted 26 January 2006)

Available online at www.sciencedirect.com
SCIENCE DIRECT®
Neuroscience Research 55 (2006) 28–33
Neuroscience Research
www.elsevier.com/locate/neures

Short-term potentiation at the parallel fiber–Purkinje cell synapse

Jun-Ichi Goto [a,b], Takafumi Inoue [a,c,*], Akinori Kuruma [a,b], Katsuhiko Mikoshiba [a,b,c]

[a] *Division of Molecular Neurobiology, The Institute of Medical Science, The University of Tokyo, 4-6-1 Shirokanedai, Minato-ku, Tokyo 108-8639 Japan*
[b] *Laboratory for Developmental Neurobiology, Brain Science Institute, RIKEN, 2-1 Hirosawa, Wako, Saitama 351-0198, Japan*
[c] *Calcium Oscillation Project, ICORP, Japan Science and Technology Corporation (JST), 3-14-4 Shirokanedai, Minato-ku, Tokyo 108-0071, Japan*

Received 6 January 2006; accepted 12 January 2006
Available online 10 February 2006

Abstract

Changes in synaptic efficacy at the parallel fiber (PF)–Purkinje cell (PC) synapse are postulated to be a cellular basis for motor learning. Although long-term efficacy changes lasting more than an hour at this synapse, i.e., long-term potentiation and depression, have been extensively studied, relatively short lasting synaptic efficacy changes, namely short-term potentiation (STP) lasting for tens of minutes, have not been discussed to date. Here we report that this synapse shows an apparent STP reliably by a periodic burst pattern of homosynaptic stimulation. This STP is presynaptically expressed, since it accompanies with a reduced paired-pulse facilitation and is resistant to postsynaptic Ca^{2+} reduction by BAPTA injection or in P/Q-type Ca channel knockout cerebella. This novel type of synaptic plasticity at the PF–PC synapse would be a clue for understanding the presynaptic mechanisms of plasticity at this synapse.

Keywords: Short-term potentiation; Purkinje cell; Parallel fiber; Synaptic plasticity; Electrophysiology; Cerebellum; Brain slice

1. Introduction

Plastic changes in synaptic efficacy are considered to be the cellular level of expression of the brain function, namely learning and memory. Long-term potentiation (LTP) of synaptic efficacy of excitatory synaptic potentials (EPSPs) at the Shaffer collateral and pyramidal cell synapse in the hippocampus CA1 area is one of the most extensively studied models for synaptic plasticity. In this synapse, potentiation induced by high frequency stimulation has been classified into three phases. Post-tetanic potentiation (PTP) is characterized by its shortest duration, terminating within seconds (Zucker and Regehr, 2002), which is followed by short-term potentiation (STP) lasting for 30-60 min. LTP follows STP, and lasts for hours to days. The nature of STP and the relationships between STP and LTP are still under debate. One hypothesis suggests that STP is a premature form of LTP in which LTP-induction stimulation was not enough to drive the plastic changes to a stable state (Gustafsson and Wigstrom, 1990; Hanse and Gustafsson, 1994). Another view is that the transient phase (STP) does not share cellular mechanisms with LTP (Schulz and Fitzgibbons, 1997; Volianskis and Jensen, 2003). The mechanistic nature and its role in synaptic encoding of STP in the CA1 pyramidal cell are unknown, which are awaited for the theories of memory retention and encoding (Albright et al., 2000).

The cerebellar cortex has been suggested to include an essential circuit for certain forms of motor learning, including associative eyeblink conditioning and adaptation of the vestibulo-ocular reflex. One cellular model system thought to contribute to learning in this structure is cerebellar long-term depression (LTD) in which coactivation of inferior olivary (climbing fiber) and granule cell (parallel fiber; PF) inputs to a Purkinje cell (PC) induces a persistent, input-specific depression of the PF–PC synapse (Ito, 2001). The converse phenomenon, cerebellar long-term potentiation (LTP), has also been described in which PF–PC synapses are strengthened by repetitive PF stimulation at low frequencies (Sakurai, 1987, 1990; Hirano, 1990, 1991; Crepel and Jaillard, 1991; Shibuki and Okada, 1992; Salin et al., 1996; Linden, 1997, 1998; Kimura et al., 1998; Storm et al., 1998; Linden and Ahn, 1999; Jacoby et al., 2001; Lev-Ram et al., 2002). In recent years, the molecular bases of cerebellar LTP have begun to be revealed. During sustained stimulation at 2–8 Hz, Ca^{2+} influx into

* Corresponding author. Tel.: +81 3 5449 5320; fax: +81 3 5449 5420.
E-mail address: tinoue@ims.u-tokyo.ac.jp (T. Inoue).

0168-0102/$ – see front matter
doi:10.1016/j.neures.2006.01.001

presynaptic terminals activates PKA through activation of the Ca/calmodulin-sensitive adenylate cyclase and production of cAMP (Salin et al., 1996; Linden, 1997; Chavis et al., 1998; Linden and Ahn, 1999; Jacoby et al., 2001). An active zone protein RIM1α has been shown to be a potent target of PKA for LTP induction at this synapse (Castillo et al., 2002; Lonart et al., 2003). Besides this presynaptic LTP, Lev-Ram et al. (2002) reported a postsynaptic form of LTP, which depends on nitric oxide, induced by 1 Hz PF stimulation at the PF–PC synapse.

Compared with the rather accumulated knowledge about the molecular basis of LTP at the PF–PC synapse, nothing has been discussed so far about potentiation of synaptic efficacy lasting a middle range of period, i.e., tens of minutes, like STP at the CA3–CA1 synapse. Here we report that PF–PC synapse shows STP which lasts 20–30 min reliably by a periodic burst pattern (five shocks at 50 Hz at a frequency of 1 Hz for 90 s). This form of synaptic plasticity would be a clue for understanding the presynaptic mechanisms of plasticity at this synapse.

2. Materials and methods

2.1. Preparation of cerebellar slices

Parasagittal cerebellar slices were prepared from 14–17 days old C57BL/6J mice (CLEA Japan Inc., Japan) or homozygous P/Q-type Ca channel (α_{1A} subunit) knock out mice (F7–F9 hybrid of 129 and C57BL/6J lines; Kulik et al., 2004) of either sex. Standard techniques were used to prepare 250 μm thick parasagittal cerebellar slices (Kuruma et al., 2003) using a vibratome-type tissue slicer (Leica Microsystems, Germany). Slices were incubated for 30 min at 37 °C and then kept at room temperature until recording, in the artificial cerebro-spinal fluid (ACSF) containing (in mM) 124 NaCl, 2.5 KCl, 2 $CaCl_2$, 2 $MgCl_2$, 1.25 NaH_2PO_4, 20 D-glucose, 26 $NaHCO_3$ and saturated with 95% O_2 and 5% CO_2. All experimental procedures were performed in accordance with the instructions of the Institute of Medical Science, The University of Tokyo for animal care and use.

2.2. Electrophysiology

Slices were transferred to recording chamber and continuously superfused with ACSF containing 10 μM bicuculline methochloride (Tocris, UK) at 2.5 ml/min, 30–32 °C. Visually guided patch clamp methods are described previously (Kuruma et al., 2003). Patch pipettes were pulled with an open tip resistance of 3–6 MΩ when filled with an internal pipette solution containing (in mM) 140 K-gluconate, 10 Hepes, 4 NaCl, 4 MgATP, 0.3 NaGTP, 0.2 bis-fura-2, and pH was adjusted to 7.3. For the experiment of intracellular infusion of BAPTA, 20 mM BAPTA (Sigma–Aldrich Co., USA) was added to the pipette solution prior to the pH adjustment. Osmolarity of internal solutions was adjusted between 280 and 290 mOsm.

Tightly sealed patch membrane was ruptured and the membrane potentials were recorded in current clamp mode using an Axoclamp 2B amplifier (Molecular Devices Corp., USA). Membrane potentials were kept at −65 mV by injecting negative currents. Experiments were rejected if the holding current exceeded −650 pA, or the junction potential drift was greater than ±5 mV, or the access resistance exceeded 25 MΩ. Input resistances were 120 MΩ to more than 1 GΩ. Initial access resistances were varied among 10–20 MΩ, and continuously compensated during recording periods. PF–PC synaptic responses were evoked with a glass electrode with an open tip of 1–3 μm, filled with ACSF, placed on the surface of the distal part of molecular layer of slices.

Excitatory postsynaptic potentials (EPSPs) were evoked at 0.2 Hz by constant-current pulses of 5–20 μA for 200 μs. Prior to each PF stimulus, a hyperpolarizing current pulse was injected through the patch pipette to monitor the series and input resistances and also to prevent cell firing, and the peak amplitude of EPSP was compensated by fitting hyperpolarizing Vm curve with a single exponential function.

After a stable baseline recording of EPSPs (4–10 mV in amplitudes), STP was induced by 90 trains of five shocks at 50 Hz at a frequency of 1 Hz. During the STP inducing stimuli were applied, membrane current was recorded in the voltage clamp mode at −60 mV and simultaneous Ca^{2+} imaging was performed. In BAPTA infusion experiments, STP was induced more than 15 min after whole-cell rupture. Cells with unstable baseline recording (>±5% deviation of the normalized EPSP in any of each 2 min recording during a 6 min baseline period in PPF and BAPTA experiments and during 10 min in other experiments) were excluded from the analysis.

2.3. Paired-pulse facilitation

Paired-pulse facilitation was measured before and after the STP induction: just prior to STP induction and at 5, 10, 15 and 20 min after the STP induction.

Each PPF test consisted of five trains of paired pulse of 80 ms interval separated by 5 s. EPSC was used as an index of synaptic strength in the PPF experiment, because measuring synaptic strength as EPSC in voltage-clamp mode has the merit to suppress voltage-activated currents which would bias especially the amplitude of facilitated second synaptic response to a pair of stimuli. However, we preferred the EPSP amplitude as an index for the long-term changes in synaptic efficacy, because EPSC amplitude is more sensitive to changes in the series resistance.

2.4. Fluorescence imaging of calcium concentration

Cytosolic Ca^{2+} concentration changes were measured by fluorescence changes of bis-fura-2 loaded through patch pipettes. Detailed methods were described previously (Kuruma et al., 2003) with a difference in a CCD camera type. An ORCA ER (Hamamatsu Photonics, Japan) was used as a detector. Ca^{2+} imaging was performed only during the STP-induction stimulation. Bis-fura-2 was loaded from the cell body for at least 20 min, and after stable baseline of EPSP was recorded, focus of microscope was adjusted on a part of dendrite close to the tip of stimulating electrode by means of bis-fura-2 fluorescence. Soon after, the STP-inducing stimuli were applied. A set of three consecutive image stacks each of which covers each Ca^{2+} transient evoked by a train of 50 Hz stimuli was taken every 29 s, and the total 12 fluorescence image stacks were used to create an averaged image to improve S/N ratio, and rectangular regions of interest (ROIs) of proper size were placed on the dendritic area. Fluorescence intensities (F) included in each ROI were averaged to represent fluorescence signal of the ROI. Ca^{2+} signals were represented by $\Delta F/F_0$, where F_0 is F of the first frame and ΔF is $F - F_0$, to normalize uneven distribution of chromophore. ROI positions were determined as to maximize the Ca^{2+} transient. When amplitude of evoked Ca^{2+} transient was smaller than 3 × S.D. of the baseline signal, the record was omitted from the analysis.

2.5. Data analysis

Electrophysiological and Ca^{2+} imaging data were acquired and analyzed using custom software TI workbench (written by T.I.).

All the data are expressed as mean ± S.E.M.

3. Results

We examined the effect of periodic burst stimuli at the PF–PC synapse in acute mouse cerebellar slice. Ninety trains of periodic bursts, which consist of five pulses at 50 Hz PF stimuli, at a frequency of 1 Hz resulted in a robust potentiation in synaptic efficacy which lasted for 10–20 min (Fig. 1). EPSP amplitudes were increased to 139.4 ± 5.6% of baseline 5 min after the burst stimulation (Fig. 1B, $n = 12$), which gradually decayed and returned to the baseline level after 20 min. This

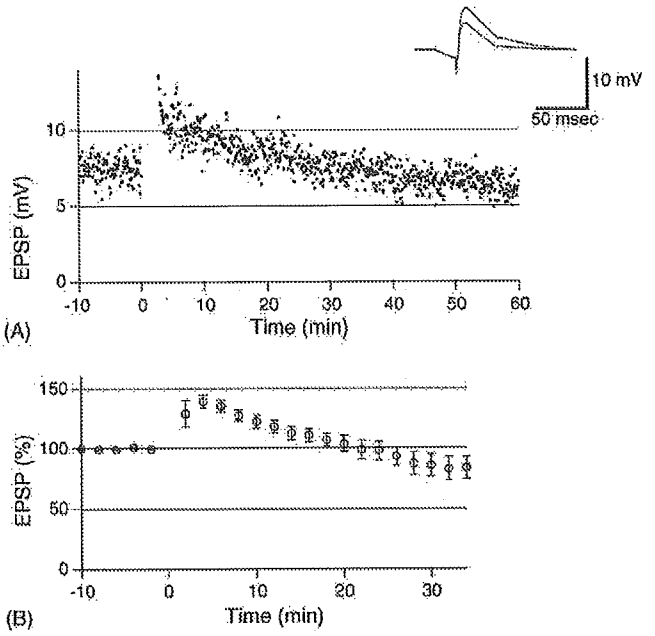

Fig. 1. Periodic burst stimuli induced STP at the PF–PC synapse which lasted 20–30 min. PF burst stimuli were applied after 10 min of stable baseline recording, and changes in EPSP amplitude were recorded thereafter. Monitoring EPSP amplitudes was done at 0.2 Hz throughout the recordings. (A) A representative trace of STP. Inset shows two overlaid EPSP traces before and 5 min after the STP induction each of which is an average trace of consecutive 24 traces (2 min). Apparent potentiation in EPSP amplitude is shown, while preceding overlapping hyperpolarizations induced by constant negative current injections indicate no apparent change in the postsynaptic membrane conductance. (B) Averaged result. Each data point shows mean normalized EPSP amplitude ± S.E.M. of consecutive 2 min records ($n = 12$).

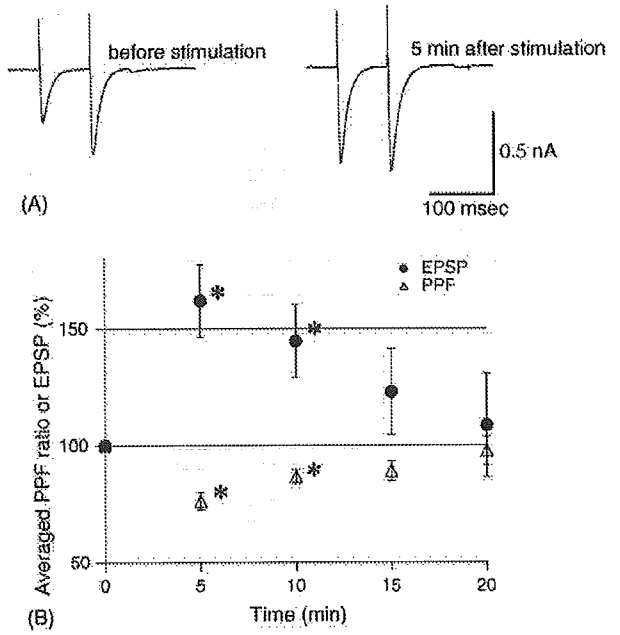

Fig. 2. Paired pulse ratio decreased in accordance with EPSP potentiation, and gradually recovered in parallel with the decay of STP. (A) Representative traces of EPSCs in response to a pair of PF stimuli separated by 80 ms recorded before and 5 min after PF short burst stimulation. (B) Time course of EPSP amplitude and paired pulse ratio. Paired pulse ratio decreased after STP induction and gradually returned to the baseline level by 20 min. This time course was almost in parallel with that of change in EPSP. $^{*}P < 0.01$, compared with the value at time zero (just before STP induction), paired t-test, $n = 5$.

periodic burst stimulation is similar to the stimulation protocol used for LTD induction at PF–PC synapse in rat cerebellar slices (Eilers et al., 1997), however, we detected only slight depression (~90% of baseline on average) at 30 min after the periodic burst stimulation.

To distinguish whether the observed STP is expressed at pre- or postsynapse, we measured paired-pulse facilitation (PPF) before and after the short burst stimuli. Paired-pulse facilitation is associated with a residual Ca^{2+} transient in the PF terminal after the first action potential (Atluri and Regehr, 1998) and an increase in transmitter release (Zucker and Regehr, 2002). Changes in the paired pulse ratio of the second pulse to the first can be affected by known modulators of transmitter release and are generally taken to reflect changes in the release probability (Dittman and Regehr, 1996). Paired pulse ratio was significantly decreased after the burst stimuli (Fig. 2, $P < 0.01$ at 5 and 10 min after stimuli, compared with the paired pulse ratio taken just before the burst stimuli, paired t-test, $n = 5$). Paired pulse ratio returned to the baseline level 20 min after the burst stimuli in parallel with the decay of the increased amplitude of EPSPs. These results suggest that presynaptic mechanisms, which affect the paired pulse ratio, underlie the observed STP at least to some extent.

Next we examined the contribution of Ca^{2+} dependent mechanism to the generation of STP. In hippocampal CA3–CA1 synapses, STP requires *N*-methyl-D-aspartate (NMDA) receptor mediated postsynaptic Ca^{2+} elevation (Malenka and Nicoll, 1993). As PCs do not express functional NMDA receptors (Konnerth et al., 1990; Perkel et al., 1990; Farrant and Cull-Candy, 1991), voltage-gated Ca channels may play a pivotal role for regulation of cytoplasmic Ca^{2+} dynamics in PC dendrites (Kuruma et al., 2003; Hartmann and Konnerth, 2005). To investigate the involvement of Ca^{2+} signals in the induction of STP, we tested the effect of ablation of P/Q-type Ca channel, which is the major subtype of voltage-gated Ca channel expressed in PC (Usowicz et al., 1992). PF–PC synapses of mouse with disrupted α1A genes, encoding a pore-forming subunit of P/Q-type Ca channel, showed almost the same time course of STP induction and decay over 10–20 min (Fig. 3A). During the STP induction period, amplitudes of Ca^{2+} transients evoked by each PF burst were measured in PC dendrites (see Section 2). Since severe reduction in Ca^{2+} transient evoked by the STP inducing stimuli was detected in knockout PC dendrites ($8.3 \pm 1.2\%$ in wild type and $3.8 \pm 0.5\%$ in $\Delta F/F$ in mutants, $P < 0.05$, Mann–Whitney test, $n = 9$ and 3, respectively), it may be less plausible that the postsynaptic Ca^{2+} changes play a major role in the STP expression.

To further examine whether the postsynaptic Ca^{2+} take a part in the expression of STP, we inhibited postsynaptic Ca^{2+} changes by loading Ca^{2+} chelator BAPTA (20 mM) through patch pipettes, which condition totally blocks postsynaptically expressed LTD at the PF–PC synapse (Konnerth et al., 1992;

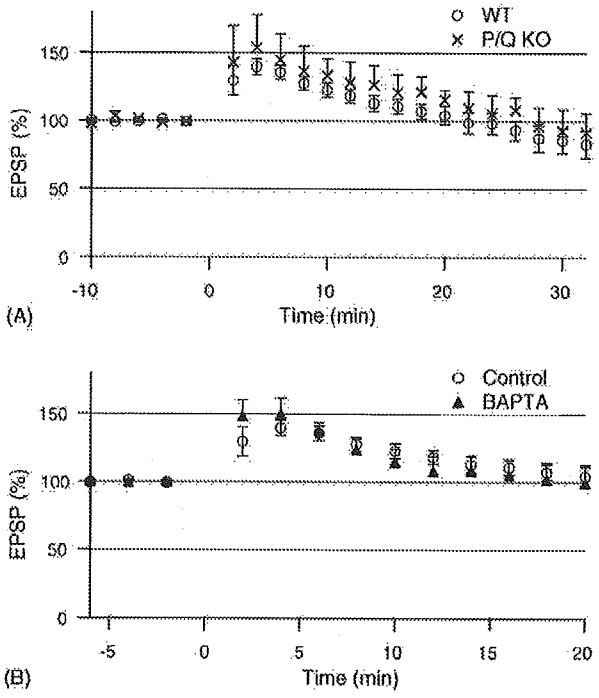

Fig. 3. Inhibition of postsynaptic Ca^{2+} did not affect the amplitude and time course of STP. (A) P/Q-type Ca channel knockout mouse. The PF–PC synapse of P/Q-type Ca channel knock out mice ($n = 3$) showed similar time course and amplitude of EPSP changes as those of wild type ($n = 12$, same trace as shown in Fig. 1B). (B) Postsynaptic BAPTA infusion. Postsynaptic BAPTA infusion (20 mM; $n = 5$) had no obvious effect on the amplitude and overall time course of STP. Averaged STP time course of wild type is overlaid ($n = 12$, same data set as shown in Fig. 1B).

Reynolds and Hartell, 2000) while presynaptically expressed LTP unaffected (Salin et al., 1996). After STP inducing short burst PF stimulation, EPSP amplitude was increased by 149 ± 12% of baseline and gradually decayed in a time course similar to that of control experiments (Fig. 3B). This result further suggests that STP is independent of postsynaptic Ca^{2+} dependent mechanisms. All the results suggest that STP induced by the short burst stimuli at PF–PC synapse is expressed presynaptically.

4. Discussion

We have shown here that repeated burst stimuli at the PF–PC synapse result in potentiation in synaptic efficacy lasting for 20–30 min. Such "short-term potentiation" of a range of 10–30 min has been well characterized at the Schaffer collaterals and pyramidal cell synapse in the hippocampus CA1 area, where STP is phenomenologically isolated from much shorter PTP of second-long (Zucker and Regehr, 2002) and from much longer LTP which lasts more than hours (Volianskis and Jensen, 2003). STP has been related to an early phase of LTP (Gustafsson and Wigstrom, 1990; Malenka, 1991; Colino et al., 1992; Hanse and Gustafsson, 1994; Xie et al., 1996), or STP and LTP have been considered as reflections of two distinct phenomena (Kauer et al., 1988; Schulz and Fitzgibbons, 1997; Volianskis and Jensen, 2003). The mechanistic nature and its role of STP in the hippocampus CA1 area are thus still under debate.

The mossy fiber–pyramidal cell synapse in the hippocampus CA3 region is also extensively studied for LTP, however, existence of STP-like synaptic efficacy change has been rarely discussed in this synapse. Exceptionally, mossy fiber synapse from mice lacking genes encoding Rab3A (Castillo et al., 1997) or RIM1α (Castillo et al., 2002) lacks LTP and potentiated synaptic efficacy returns to the basal level within 10–20 min. The PF–PC synapse shares some features with the mossy fiber–pyramidal cell synapse. Both synapses show presynaptically expressed PKA-dependent LTP (Nicoll and Malenka, 1995; Salin et al., 1996; Linden, 1997; Chavis et al., 1998; Linden and Ahn, 1999; Jacoby et al., 2001). And further, the PF–PC LTP also depends on RIM1α, as it returns to the baseline within 10–20 min in RIM1α knockout mice (Castillo et al., 2002). Without this exception, there has been no report about STP-like synaptic potentiation which decays over 20–30 min in the PF–PC synapse. If STP revealed in this study share molecular mechanisms with the LTP induction in this synapse, the STP induction protocol employed in this study might be a clue to dissect the molecular mechanisms of early steps of LTP induction at PF–PC synapse. Or it would be also interesting if STP found in this study is a distinct phenomenon from LTP.

We revealed that STP found in this study is presynaptically expressed according to the following observations. Firstly, STP was accompanied by a decrease in paired pulse ratio with a similar recovery time course (Fig. 2B). Changes in the paired pulse ratio of the second pulse to the first are generally taken to reflect changes in the release probability (Dittman and Regehr, 1996). Secondly, STP was not affected by postsynaptic BAPTA loading which blocks postsynaptic Ca^{2+} dependent events (Fig. 3B). Finally STP was similarly observed in P/Q-type Ca channel knockout mice (Fig. 3A), in which amplitudes of postsynaptic Ca^{2+} transients evoked by the STP-inducing stimulation were apparently reduced (see Section 3). Whether or not this STP and presynaptically expressed LTP are reflections of a single process of potentiation that includes multiple phases or whether this STP and the LTP are distinct phenomena remained to be elucidated.

Eilers et al. (1997) reported a homosynaptic LTD at the PF–PC synapse by a similar stimulation pattern as used in this study. Two to five pulses at 10–50 Hz at a frequency of 1 Hz for 1–2 min resulted in a robust depression of PF synaptic responses (58%). We did not observe such a robust long-lasting depression of PF responses in this study (~90% of baseline 30 min after the induction) with five pulses at 50 Hz at a frequency of 1 Hz for 1.5 min, but did observe STP. Differences in the experimental conditions may explain the different results: mouse was used in this study and rat in the other, and the bath temperature was 30–32 °C in this study and 20–22 °C in the other. Nevertheless, we do not consider that the STP observed in this study is simply an overlap of postsynaptic LTD and presynaptic LTP, because STP was not affected by postsynaptic loading of BAPTA (Fig. 3B) and the time course of paired pulse ratio change was in accordance with that of synaptic efficacy change (Fig. 2B).

The stimulation pattern for induction of STP employed in this study was different from the LTP-inducing stimulation patterns employed in recent studies in that the former is composed of periodic burst of 50 Hz trains and the latter uses evenly spaced pulses at 2–8 Hz (Salin et al., 1996; Linden, 1997; Chavis et al., 1998; Linden and Ahn, 1999; Jacoby et al., 2001). Although the averaged numbers of stimuli of the both stimulations fall in the same range (5 times/s versus 2–8 Hz), bursting action potentials at the PF terminal might result in much higher accumulation of Ca^{2+} in presynapse which would result in a different consequence, i.e., STP, from the slow and evenly spaced arrival of action potentials. Since the firing frequency of cerebellar granule cells is around 10–50 Hz at resting and increased by 50–100 Hz under sensory stimulations recorded in vivo (Ito, 2001; Chadderton et al., 2004), the periodic bursting PF stimuli employed in this study may represent a physiologically occurring firing pattern.

Acknowledgements

We thank Dr. Chihiro Hisatsune for discussions and Mr. Akira Futatsugi and Mses. Etsuko Ebisui and Mizuki Yamada for breeding the mutant mice.

References

Albright, T.D., Jessell, T.M., Kandel, E.R., Posner, M.I., 2000. Neural science: a century of progress and the mysteries that remain. Cell 100 (Suppl.), S1–S55.

Atluri, P.P., Regehr, W.G., 1998. Delayed release of neurotransmitter from cerebellar granule cells. J. Neurosci. 18, 8214–8227.

Castillo, P.E., Janz, R., Sudhof, T.C., Tzounopoulos, T., Malenka, R.C., Nicoll, R.A., 1997. Rab3A is essential for mossy fibre long-term potentiation in the hippocampus. Nature 388, 590–593.

Castillo, P.E., Schoch, S., Schmitz, E., Sudhof, T.C., Malenka, R.C., 2002. RIM1α is required for presynaptic long-term potentiation. Nature 415, 327–330.

Chadderton, P., Margrie, T.W., Hausser, M., 2004. Integration of quanta in cerebellar granule cells during sensory processing. Nature 428, 856–860.

Chavis, P., Mollard, P., Bockaert, J., Manzoni, O., 1998. Visualization of cyclic AMP-regulated presynaptic activity at cerebellar granule cells. Neuron 20, 773–781.

Colino, A., Huang, Y.Y., Malenka, R.C., 1992. Characterization of the integration time for the stabilization of long-term potentiation in area CA1 of the hippocampus. J. Neurosci. 12, 180–187.

Crepel, R., Jaillard, D., 1991. Pairing of pre- and postsynaptic activities in cerebellar Purkinje cells induces long-term changes in synaptic efficacy in vitro. J. Physiol. 432, 123–141.

Dittman, J.S., Regehr, W.G., 1996. Contributions of calcium-dependent and calcium-independent mechanisms to presynaptic inhibition at a cerebellar synapse. J. Neurosci. 16, 1623–1633.

Eilers, J., Takechi, H., Finch, E.A., Augustine, G.J., Konnerth, A., 1997. Local dendritic Ca^{2+} signaling induces cerebellar long-term depression. Learn. Mem. 4, 159–168.

Farrant, M., Cull-Candy, S.G., 1991. Excitatory amino acid receptor-channels in Purkinje cells in thin cerebellar slices. Proc. Biol. Sci. 244, 179–184.

Gustafsson, B., Wigstrom, H., 1990. Long-term potentiation in the hippocampal CA1 region: its induction and early temporal development. Prog. Brain. Res. 83, 223–232.

Hanse, E., Gustafsson, B., 1994. Onset and stabilization of NMDA receptor-dependent hippocampal long-term potentiation. Neurosci. Res. 20, 15–25.

Hartmann, J., Konnerth, A., 2005. Determinants of postsynaptic Ca^{2+} signaling in Purkinje neurons. Cell Calcium 37, 459–466.

Hirano, T., 1990. Depression and potentiation of the synaptic transmission between a granule cell and a Purkinje cell in rat cerebellar culture. Neurosci. Lett. 119, 141–144.

Hirano, T., 1991. Synaptic formations and modulations of synaptic transmissions between identified cerebellar neurons in culture. J. Physiol. (Paris) 85, 145–153.

Ito, M., 2001. Cerebellar long-term depression: characterization, signal transduction, and functional roles. Physiol. Rev. 81, 1143–1195.

Jacoby, S., Sims, R.E., Hartell, N.A., 2001. Nitric oxide is required for the induction and heterosynaptic spread of long-term potentiation in rat cerebellar slices. J. Physiol. 535, 825–839.

Kauer, J.A., Malenka, R.C., Nicoll, R.A., 1988. NMDA application potentiates synaptic transmission in the hippocampus. Nature 334, 250–252.

Kimura, S., Uchiyama, S., Takahashi, H.E., Shibuki, K., 1998. cAMP-dependent long-term potentiation of nitric oxide release from cerebellar parallel fibers in rats. J. Neurosci. 18, 8551–8558.

Konnerth, A., Llano, I., Armstrong, C.M., 1990. Synaptic currents in cerebellar Purkinje cells. Proc. Natl. Acad. Sci. U.S.A. 87, 2662–2665.

Konnerth, A., Dreessen, J., Augustine, G.J., 1992. Brief dendritic calcium signals initiate long-lasting synaptic depression in cerebellar Purkinje cells. Proc. Natl. Acad. Sci. U.S.A. 89, 7051–7055.

Kulik, A., Nakadate, K., Hagiwara, A., Fukazawa, Y., Lujan, R., Saito, H., Suzuki, N., Futatsugi, A., Mikoshiba, K., Frotscher, M., Shigemoto, R., 2004. Immunocytochemical localization of the α1A subunit of the P/Q-type calcium channel in the rat cerebellum. Eur. J. Neurosci. 19, 2169–2178.

Kuruma, A., Inoue, T., Mikoshiba, K., 2003. Dynamics of Ca^{2+} and Na^{+} in the dendrites of mouse cerebellar Purkinje cells evoked by parallel fibre stimulation. Eur. J. Neurosci. 18, 2677–2689.

Lev-Ram, V., Wong, S.T., Storm, D.R., Tsien, R.Y., 2002. A new form of cerebellar long-term potentiation is postsynaptic and depends on nitric oxide but not cAMP. Proc. Natl. Acad. Sci. U.S.A. 99, 8389–8393.

Linden, D.J., 1997. Long-term potentiation of glial synaptic currents in cerebellar culture. Neuron 18, 983–994.

Linden, D.J., 1998. Synaptically evoked glutamate transport currents may be used to detect the expression of long-term potentiation in cerebellar culture. J. Neurophysiol. 79, 3151–3156.

Linden, D.J., Ahn, S., 1999. Activation of presynaptic cAMP-dependent protein kinase is required for induction of cerebellar long-term potentiation. J. Neurosci. 19, 10221–10227.

Lonart, G., Schoch, S., Kaeser, P.S., Larkin, C.J., Sudhof, T.C., Linden, D.J., 2003. Phosphorylation of RIM1α by PKA triggers presynaptic long-term potentiation at cerebellar parallel fiber synapses. Cell 115, 49–60.

Malenka, R.C., 1991. Postsynaptic factors control the duration of synaptic enhancement in area CA1 of the hippocampus. Neuron 6, 53–60.

Malenka, R.C., Nicoll, R.A., 1993. NMDA-receptor-dependent synaptic plasticity: multiple forms and mechanisms. Trends Neurosci. 16, 521–527.

Nicoll, R.A., Malenka, R.C., 1995. Contrasting properties of two forms of long-term potentiation in the hippocampus. Nature 377, 115–118.

Perkel, D.J., Hestrin, S., Sah, P., Nicoll, R.A., 1990. Excitatory synaptic currents in Purkinje cells. Proc. Biol. Sci. 241, 116–121.

Reynolds, T., Hartell, N.A., 2000. An evaluation of the synapse specificity of long-term depression induced in rat cerebellar slices. J. Physiol. 527 (Pt 3), 563–577.

Sakurai, M., 1987. Synaptic modification of parallel fibre–Purkinje cell transmission in in vitro guinea-pig cerebellar slices. J. Physiol. 394, 463–480.

Sakurai, M., 1990. Calcium is an intracellular mediator of the climbing fiber in induction of cerebellar long-term depression. Proc. Natl. Acad. Sci. U.S.A. 87, 3383–3385.

Salin, P.A., Malenka, R.C., Nicoll, R.A., 1996. Cyclic AMP mediates a presynaptic form of LTP at cerebellar parallel fiber synapses. Neuron 16, 797–803.

Schulz, P.E., Fitzgibbons, J.C., 1997. Differing mechanisms of expression for short-and long-term potentiation. J. Neurophysiol. 78, 321–334.

Shibuki, K., Okada, D., 1992. Cerebellar long-term potentiation under suppressed postsynaptic Ca^{2+} activity. Neuroreport 3, 231–234.

Storm, D.R., Hansel, C., Hacker, B., Parent, A., Linden, D.J., 1998. Impaired cerebellar long-term potentiation in type I adenylyl cyclase mutant mice. Neuron 20, 1199–1210.

Usowicz, M.M., Sugimori, M., Cherksey, B., Llinas, R., 1992. P-type calcium channels in the somata and dendrites of adult cerebellar Purkinje cells. Neuron 9, 1185–1199.

Volianskis, A., Jensen, M.S., 2003. Transient and sustained types of long-term potentiation in the CA1 area of the rat hippocampus. J. Physiol. 550, 459–492.

Xie, X., Barrionuevo, G., Berger, T.W., 1996. Differential expression of short-term potentiation by AMPA and NMDA receptors in dentate gyrus. Learn. Mem. 3, 115–123.

Zucker, R.S., Regehr, W.G., 2002. Short-term synaptic plasticity. Annu. Rev. Physiol. 64, 355–405.

Available online at www.sciencedirect.com
SCIENCE DIRECT
ELSEVIER
Biochemical and Biophysical Research Communications 342 (2006) 573–576
BBRC
www.elsevier.com/locate/ybbrc

4.1N binding regions of inositol 1,4,5-trisphosphate receptor type 1 ☆

Kazumi Fukatsu [a,b], Hiroko Bannai [b,1], Takafumi Inoue [a,c,*], Katsuhiko Mikoshiba [a,b,c]

[a] *Division of Molecular Neurobiology, The Institute of Medical Science, The University of Tokyo, Tokyo 108-8639, Japan*
[b] *Laboratory for Developmental Neurobiology, Brain Science Institute, RIKEN, Saitama 351-0198, Japan*
[c] *Calcium Oscillation Project, ICORP-SORST, Japan Science and Technology Agency (JST), Saitama 332-0012, Japan*

Received 31 January 2006
Available online 10 February 2006

Abstract

Zhang et al. and Maximov et al. [S. Zhang, A. Mizutani, C. Hisatsune, T. Higo, H. Bannai, T. Nakayama, M. Hattori, and K. Mikoshiba, Protein 4.1N is required for translocation of inositol 1,4,5-trisphosphate receptor type 1 to the basolateral membrane domain in polarized Madin-Darby canine kidney cells, J. Biol. Chem. 278 (2003) 4048–4056; A. Maximov, T. S. Tang, and I. Bezprozvanny, Association of the type 1 inositol (1,4,5)-trisphosphate receptor with 4.1N protein in neurons, Mol. Cell. Neurosci. 22 (2003) 271–283.] reported that 4.1N is a binding partner of inositol 1,4,5-trisphosphate receptor type 1 (IP_3R1), however the binding site of IP_3R1 differed: the former determined the C-terminal 14 amino acids of the cytoplasmic tail (CTT14aa) as the binding site, while the latter assigned another segment, cytoplasmic tail middle 1 (CTM1). To solve this discrepancy, we performed immunoprecipitation and found that both the segments had binding activity to 4.1N. Both segments also interfered the 4.1N-regulated IP_3R1 diffusion in neuronal dendrites. However, IP_3R1 lacking the CTT14aa (IP_3R1-ΔCTT14aa) does not bind to 4.1N [S. Zhang, A. Mizutani, C. Hisatsune, T. Higo, H. Bannai, T. Nakayama, M. Hattori, and K. Mikoshiba, Protein 4.1N is required for translocation of inositol 1,4,5-trisphosphate receptor type 1 to the basolateral membrane domain in polarized Madin-Darby canine kidney cells, J. Biol. Chem. 278 (2003) 4048–4056.] and its diffusion constant is larger than that of IP_3R1 full-length in neuronal dendrites [K. Fukatsu, H. Bannai, S. Zhang, H. Nakamura, T. Inoue, and K. Mikoshiba, Lateral diffusion of inositol 1,4,5-trisphosphate receptor type 1 is regulated by actin filaments and 4.1N in neuronal dendrites, J. Biol. Chem. 279 (2004) 48976–48982.]. We conclude that both the CTT14aa and CTM1 sequences can bind to 4.1N in peptide fragment forms. However, we propose that the responsible binding site for 4.1N binding in full-length tetramer form of IP_3R1 is CTT14aa.

Keywords: Inositol 1,4,5-trisphosphate receptor type 1; 4.1N; CTT14aa; CTM1; Immunoprecipitation; Diffusion

Inositol 1,4,5-trisphosphate receptors (IP_3Rs) are intracellular Ca^{2+} channels that are responsible for Ca^{2+} release from intracellular stores and located on the endoplasmic reticulum (ER) membrane [4]. Three isoforms of IP_3Rs have been identified in mammalians [5]. IP_3R type 1 (IP_3R1) is highly expressed in the central nervous system [6,7] and plays a critical role in the regulation of neuronal activities [8–12]. Recently, 4.1N, which contains an actin-spectrin binding domain, is determined as a binding partner of IP_3R1 [1,2]. 4.1N is also reported to play roles in the translocation of IP_3R, as well as in the cell surface expression of neurotransmitter receptors [13,14]. In polarized Madin-Darby canine kidney (MDCK) cells, 4.1N is required for IP_3R1 translocation to the basolateral membrane domain [1]. In neurons, the interaction of IP_3R1 and 4.1N is also thought to be important for the targeting of IP_3R1 [2]. In hippocampal neurons, we suggest that IP_3R1 diffusion on ER membrane is regulated by actin

☆ *Abbreviations:* IP_3, inositol 1,4,5-trisphosphate; IP_3R, inositol 1,4,5-trisphosphate receptor; ER, endoplasmic reticulum; IP_3R1, inositol 1,4,5-trisphosphate receptor type 1; IP_3R3, inositol 1,4,5-trisphosphate receptor type 3; FRAP, fluorescence recovery after photobleaching; GFP, green fluorescent protein; mRFP, monomeric red fluorescent protein; D_{eff}, effective diffusion constant; SD, standard deviation; PBS, phosphate-buffered saline; CTD, C-terminal domain; CTT, C-terminal cytoplasmic tail; MDCK, Madin-Darby canine kidney.

* Corresponding author. Fax: +81 3 5449 5420.
E-mail address: tinoue@ims.u-tokyo.ac.jp (T. Inoue).
[1] Present address: Biologie Cellulaire de la Synapse N & P, Ecole Normale Supérieure, INSERM U497, 46 Rue d'Ulm, 75005, Paris, France.

0006-291X/$ - see front matter © 2006 Elsevier Inc. All rights reserved.
doi:10.1016/j.bbrc.2006.02.010

filaments, and 4.1N works as a linker protein between IP_3R1 and actin filaments [3].

Maximov et al. and Zhang et al. [1,2] have reported detailed molecular interaction between 4.1N and IP_3R1. Both groups found 4.1N as one of IP_3R1 binding partners by yeast two-hybrid screen, and confirmed the binding by immunoprecipitation using entire coding sequence of both proteins. There is a point of controversy in the binding site in the IP_3R1 structure between the two groups. Maximov et al. narrowed down the binding site to an 87 amino acid stretch in the C-terminal tail (2590–2676aa; cytoplasmic tail middle 1; CTM1), while Zhang et al. confined the binding site of IP_3R1 in the C-terminal 14 amino acids (2736–2749aa; CTT14aa). Maximov et al. showed that 4.1N bound not to CTT14aa but CTM1 by yeast two-hybrid assay and further the CTM1 fragment competed with the interaction between full length-IP_3R1 and 4.1N. On the contrary, Zhang et al. showed that C-terminal fragment of IP_3R1 containing not CTM1 but CTT14aa bound to 4.1N by yeast two-hybrid assay. By means of pull-down assay, they also showed that full-length IP_3R1 or the CTT14aa peptide bound to 4.1N while an IP_3R1 mutant lacking CTT14aa did not. In addition, we have recently found that the lateral diffusion of IP_3R1 on ER membrane in neuronal dendrites is regulated by interaction with 4.1N through CTT14aa [3]. In order to clarify this controversy, whether CTT14aa and/or CTM1 is (are) needed for the interaction between IP_3R1 and 4.1N, we performed experiments which directly compare both the elements of IP_3R1 in the context of 4.1N–IP_3R1 interaction.

Materials and methods

DNA constructions. All PCR products were verified by nucleotide sequencing using an ABI 3130 Genetic Analyzer (Applied Biosystems, Foster City, USA). A monomeric red fluorescent protein (mRFP) expression plasmid (pcDNA3.1/Zeo+-mRFP) was generated by inserting a fragment encoding mRFP [15], which was kindly provided by Dr. Tsien (University of California, San Diego, USA), into the *Eco*RI–*Bam*HI site of pcDNA3.1/Zeo+ (Invitrogen, Tokyo, Japan).

DNA fragments corresponding to aa 2590–2677 (CTM1), 2677–2735 (CTM2), and 2677–2749 (CTM2-CTT14aa) of mouse IP_3R1 were amplified by PCR.

The mRFP-tagged constructs were generated by inserting synthesized DNA fragments into the *Eco*RI–*Xho*I site of pcDNA3.1/Zeo+-mRFP.

The GFP-tagged CTM1, CTM2, and CTM2-CTT14aa were generated by replacing an ES fragment in pcDNA3.1/Zeo+GFP-IP_3R1-ES [16] with CTM1, CTM2 or CTM2-CTT14aa (*Eco*RI–*Xho*I).

Cell culture and transfection. Primary cultures of hippocampal neurons were prepared from the hippocampi of 1-day-old Wistar rats, as described previously [3]. Neurons were plated on poly-L-lysine (Nacalai Tesque, Kyoto, Japan)-coated coverslips at a density of 3.2×10^4 cells/cm^2 and cultured in Neurobasal Medium (Invitrogen) supplemented with 2.5 mM L-glutamine (Nacalai Tesque), 2.5% (v/v) B-27 (Invitrogen), and antibiotics (250 U/ml penicillin and 250 μg/ml streptomycin).

Cultures were transfected with 10 μg of the DNAs, usually on days 4–5 in vitro, using a standard calcium phosphate method [17]. The transfected cells were used for imaging experiments 1–3 days after the transfection.

Time-lapse imaging, photobleaching experiments, and estimation of the effective diffusion constant (D_{eff}). For the time-lapse imaging experiments, the culture medium was supplemented with 20 mM Hepes (pH 7.3). Fluorescence images of the cells were taken under a confocal scanning microscope (FV-300; Olympus, Tokyo, Japan) attached to an inverted microscope with a 60× objective (NA 1.4, oil immersion, UPlanApo, Olympus), as described previously [3]. The GFP signal was excited at 488 nm and emission was detected through a 510–550 nm bandpass filter. The mRFP signal was excited at 568 nm and emission was detected through a 585 nm bandpass filter.

The effective diffusion constants (D_{eff}) of GFP-IP_3R1 were quantified by the fluorescence recovery after photobleaching (FRAP) technique as was described previously [3].

Co-immunoprecipitation and immunoblotting. COS-7 cells were maintained in Dulbecco's modified Eagle's medium (Nacalai Tesque) supplemented with 10% heat-inactivated fetal bovine serum. Five micrograms of DNA/φ10 cm dish was transfected using TransIT transfection reagents (Mirus Bio Corporation, Madison, USA) according to the manufacturer's protocol. Transfected COS-7 cells were harvested one day after transfection. Lysates of transfected COS-7 cells were prepared as previously described [13]. Cell lysates were centrifuged at 10,000*g* for 30 min at 4 °C and supernatant was used for immunoprecipitation. For each reaction, 7.5 μg of anti-HA mouse monoclonal antibody (clone 12CA5, Roche, Basel, Switzerland) or anti-mouse IgG antibody (Sigma–Aldrich Japan, Tokyo, Japan) was preincubated with lysates for 1 h at 4 °C and incubated with protein G–Sepharose (GE Healthcare Bio-Sciences Corp., Piscataway, USA) 30 μl for 2–3 h at 4 °C. Then the complexes were spun down and washed with buffer for three times [13]. The proteins were eluted by boiling in 1× SDS–PAGE sample buffer for 3 min and were separated by SDS–PAGE. The proteins were transferred to a polyvinylidene difluoride (PDVF) membrane (Millipore, Bedford, USA), and the membranes were probed with anti-EGFP Ab (Santa Cruz Biotechnology, Inc., Santa Cruz, USA) and anti-HA Ab (Zymed Laboratories, San Francisco, USA).

Results and discussion

We tested binding activity of the following three sequences in IP_3R1 to 4.1N (Fig. 1A). The first is aa2590–2676, which we call CTM1, the binding sequence reported by Maximov et al. [2]. The second is aa2677–2735 (CTM2) whose binding activity to 4.1N tested by yeast two-hybrid assay was negative [2]. The last one is aa2677–2749 (CTM2-CTT14aa), which contains CTT14aa but is reported to have negative binding activity to 4.1N in yeast two-hybrid assay [2].

These sequences were fused with GFP to their N-termini, and co-expressed with HA-4.1N-FL in COS-7 cells. Cell lysates were immunoprecipitated with an anti-HA antibody or control IgG (Fig. 1B). GFP-CTM1 (GFP-tagged CTM1) bound to 4.1N, while GFP-CTM2 did not. These results are consistent with Maximov et al. However, contrary to their results of yeast two-hybrid assay, GFP-CTM2-CTT14aa (GFP-tagged CTM2-CTT14aa) also interacted with 4.1N. The inconsistency between yeast two-hybrid assay and other experiments may reflect the inherent tricky feature of the yeast two-hybrid assay [18]. We conclude that both of the previously described binding sites of IP_3R1 for 4.1N, CTM1 and CTT14aa, have binding activity to 4.1N.

We have shown that overexpression of a CTT14aa fragment had an effect on GFP-IP_3R1 diffusion in neuronal dendrites: CTT14aa increased apparent diffusion constant (D_{eff}) of IP_3R1 by interfering 4.1N-IP_3R1 binding [3]. We investigated whether CTM1 has a similar effect on the

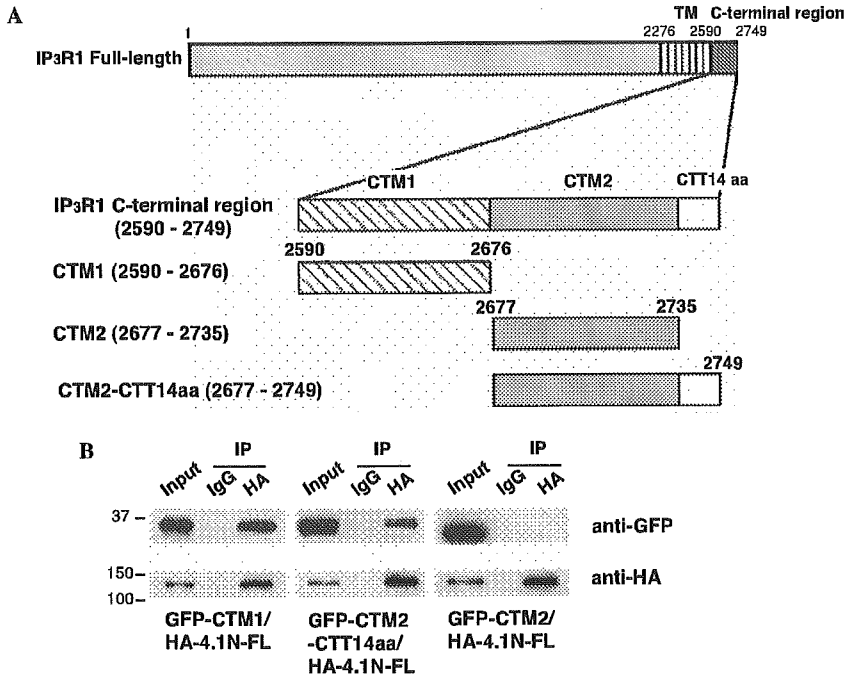

Fig. 1. The 4.1N-binding region in the IP_3 R1 carboxyl-terminal. (A) Schematic representation of the structures of full-length IP_3R1 and its cytoplasmic carboxyl-terminal regions. Full-length (aa 1–2749), CTM1 (2590–2676), CTM2-CTT14aa (2677–2749), and CTM2 (2677–2735). TM, transmembrane domain. (B) HA-4.1N-FL was transiently transfected to COS-7 cells with GFP-CTM1, GFP-CTM2-CTT14aa or GFP-CTM2, and the cell lysates were immunoprecipitated (IP) with an anti-HA antibody or control IgG. The immunoprecipitates were subjected to SDS–PAGE followed by Western blotting with anti-GFP and anti-HA antibodies. GFP-CTM1 and GFP-CTM2-CTT14aa bound to HA-4.1N-FL, but GFP-CTM2 did not.

GFP-IP_3R1 diffusion in this study. GFP-IP_3R1 was co-expressed with mRFP-tagged CTM1, CTM2 or CTM2-CTT14aa in cultured hippocampal neurons, and D_{eff} of GFP-IP_3R1 was measured (Fig. 2). D_{eff} of GFP-IP_3R1 in the control condition co-expressing mRFP was $0.28 \pm 0.07\ \mu m^2/s$ ($n = 13$). Co-expression of mRFP-CTM1 significantly increased D_{eff} of GFP-IP_3R1 to $0.34 \pm 0.06\ \mu m^2/s$ ($n = 27$). D_{eff} of GFP-IP_3R1 was also significantly increased ($0.38 \pm 0.08\ \mu m^2/s$, $n = 37$) (Fig. 2) by overexpression of mRFP-CTM2-CTT14aa, the effect of which was similar to that of mRFP-CTT14aa [3]. On the other hand, overexpression of mRFP-CTM2 did not affect the D_{eff} of GFP-IP_3R1 ($0.30 \pm 0.06\ \mu m^2/s$, $n = 17$). These results indicate that the CTM1 fragment affects the lateral diffusion of IP_3R1 as CTT14aa does (Fig. 2).

Now we draw a conclusion that both CTT14aa and CTM1 fragments have binding affinity for 4.1N. However, we propose that the responsible binding site for 4.1N binding in full-length tetramer-form of IP_3R1 is CTT14aa according to following reasons. GFP-IP_3R1-ΔCTT14aa did not bind to 4.1N in spite of including CTM1 in the immunoprecipitation experiment [1], and GFP-IP_3R1-ΔCTT14aa did not show 4.1N-dependent translocation in confluent MDCK cells [1]. D_{eff} of GFP-IP_3R1-ΔCTT14aa was larger than that of GFP-IP_3R1 and as fast as that of GFP-IP_3R3, which lacks CTT14aa sequence. Furthermore, when GFP-IP_3R3 was fused with a CTT14aa fragment, it became able to bind to 4.1N and its lateral diffusion became subjected to actin-dependent regulation [3]. All

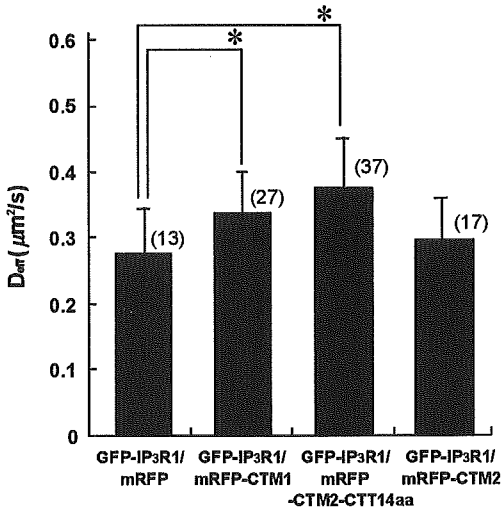

Fig. 2. CTM1 and CTT14aa are involved in the regulation of GFP-IP_3R1 diffusion. D_{eff} of GFP-IP_3R1 under co-expression with mRFP, mRFP-CTM1, mRFP-CTM2-CTT14aa or mRFP-CTM2. Data represent means ± SD $^*p < 0.05$ (t test). Numbers in parentheses indicate numbers of neurons.

these lines of evidence suggest that the CTT14aa sequence is necessary and sufficient for the IP_3R1–4.1N interaction and that 4.1N may not be able to access to CTM1, when IP_3R1 is in its native form. The fact that a monoclonal antibody 18A10, the epitope of which lies over CTT14aa,

binds to native IP_3R1 thereby blocks its channel function [19] supports the idea that the CTT14aa region of IP_3R1 is exposed and capable of association with other proteins.

Acknowledgments

We are grateful to Dr. R. Tsien (University of California, San Diego, USA) for the gift of monomeric RFP. We thank Dr. I. Bezprozvanny (University of Southwestern Medical Center, Dallas, USA) for valuable suggestion. We thank Dr. A. Mizutani, N. Matsumoto, and S. Tamamushi (University of Tokyo, Tokyo, Japan) for technical assistance. This study was supported by grants from the Ministry of Education, Culture, Sports, Science and Technology of Japan (to H.B., T.I. and K.M.), the Ministry of Health, Labour and Welfare (to T.I.), RIKEN and the 21st Century COE Program, Center for Integrated Brain Medical Science, from the Ministry of Education, Culture, Sports, Science and Technology of Japan.

References

[1] S. Zhang, A. Mizutani, C. Hisatsune, T. Higo, H. Bannai, T. Nakayama, M. Hattori, K. Mikoshiba, Protein 4.1N is required for translocation of inositol 1,4,5-trisphosphate receptor type 1 to the basolateral membrane domain in polarized Madin-Darby canine kidney cells, J. Biol. Chem. 278 (2003) 4048–4056.

[2] A. Maximov, T.S. Tang, I. Bezprozvanny, Association of the type 1 inositol (1,4,5)-trisphosphate receptor with 4.1N protein in neurons, Mol. Cell. Neurosci. 22 (2003) 271–283.

[3] K. Fukatsu, H. Bannai, S. Zhang, H. Nakamura, T. Inoue, K. Mikoshiba, Lateral diffusion of inositol 1,4,5-trisphosphate receptor type 1 is regulated by actin filaments and 4.1N in neuronal dendrites, J. Biol. Chem. 279 (2004) 48976–48982.

[4] M.J. Berridge, M.D. Bootman, H.L. Roderick, Calcium signalling: dynamics, homeostasis and remodelling, Nat. Rev. Mol. Cell Biol. 4 (2003) 517–529.

[5] T. Furuichi, K. Kohda, A. Miyawaki, K. Mikoshiba, Intracellular channels, Curr. Opin. Neurobiol. 4 (1994) 294–303.

[6] P.F. Worley, J.M. Baraban, J.S. Colvin, S.H. Snyder, Inositol trisphosphate receptor localization in brain: variable stoichiometry with protein kinase C, Nature 325 (1987) 159–161.

[7] T. Furuichi, D. Simon-Chazottes, I. Fujino, N. Yamada, Hasegawa, A. Miyawaki, S. Yoshikawa, J.L. Guenet, K. Mikosh Widespread expression of inositol 1,4,5-trisphosphate receptor ty gene (Insp3r1) in the mouse central nervous system, Recep Channels 1 (1993) 11–24.

[8] S. Fujii, M. Matsumoto, K. Igarashi, H. Kato, K. Mikosh Synaptic plasticity in hippocampal CA1 neurons of mice lacking t 1 inositol-1,4,5-trisphosphate receptors, Learn Mem. 7 (2(312–320.

[9] M. Nishiyama, K. Hong, K. Mikoshiba, M.M. Poo, K. K Calcium stores regulate the polarity and input specificity of syna modification, Nature 408 (2000) 584–588.

[10] T. Inoue, K. Kato, K. Kohda, K. Mikoshiba, Type 1 inositol 1, trisphosphate receptor is required for induction of long-term dep sion in cerebellar Purkinje neurons, J. Neurosci. 18 (1998) 5366–5

[11] H. Takechi, J. Eilers, A. Konnerth, A new class of synaptic respo involving calcium release in dendritic spines, Nature 396 (19 757–760.

[12] E.A. Finch, G.J. Augustine, Local calcium signalling by inosi 1,4,5-trisphosphate in Purkinje cell dendrites, Nature 396 (19 753–756.

[13] L. Shen, F. Liang, L.D. Walensky, R.L. Huganir, Regulation AMPA receptor GluR1 subunit surface expression by a 1N-linked actin cytoskeletal association, J. Neurosci. 20 (20 7932–7940.

[14] A.V. Binda, N. Kabbani, R. Lin, R. Levenson, D2 and D3 dopam receptor cell surface localization mediated by interaction with prot 4.1N, Mol. Pharmacol. 62 (2002) 507–513.

[15] R.E. Campbell, O. Tour, A.E. Palmer, P.A. Steinbach, G.S. Bai D.A. Zacharias, R.Y. Tsien, A monomeric red fluorescent prote Proc. Natl. Acad. Sci. USA 99 (2002) 7877–7882.

[16] T. Nakayama, M. Hattori, K. Uchida, T. Nakamura, Y. Tateishi, Bannai, M. Iwai, T. Michikawa, T. Inoue, K. Mikoshiba, T regulatory domain of the inositol 1,4,5-trisphosphate receptor necessary to keep the channel domain closed: possible physiologi significance of specific cleavage by caspase 3, Biochem. J. 377 (20 299–307.

[17] M. Köhrmann, W. Haubensak, I. Hemraj, C. Kaether, V Leßmann, M.A. Kiebler, Fast, convenient, and effective method transiently transfect primary hippocampal neurons, J. Neurosci. R 58 (1999) 831–835.

[18] S. Fields, R. Sternglanz, The two-hybrid system: an assay for prote protein interactions, Trends Genet. 10 (1994) 286–292.

[19] S. Nakade, N. Maeda, K. Mikoshiba, Involvement of the C-termi of the inositol 1,4,5-trisphosphate receptor in Ca^{2+} release analy using region-specific monoclonal antibodies, Biochem. J. 277 (Pt. (1991) 125–131.